Chapter one

Introduction

1.1 Thermo Electric Devices

In 1834, a French watchmaker and part time physicist, Jean Peltier who found that an electrical current would produce a temperature gradient at the junction of two dissimilar metals. Thermal current and electric current flow in opposite directions.

Thermoelectric devices have gained importance in recent years as viable solutions for applications such as spot cooling of electronic components, remote power generation in space stations and satellites etc.

These solid-state devices have long been known for their reliability rather than their efficiency; they contain no moving parts, and their performance relies primarily on material selection, which has not generated many excellent candidates.

Research in recent years has been focused on developing both thermoelectric Structures and materials that have high efficiency. In general, thermoelectric research is two-pronged with [1] experiments focused on finding new materials and structures with enhanced thermoelectric performance and [2] analytical models that predict thermoelectric behavior to enable better design and optimization of materials and structures. While numerous reviews have discussed the importance of and dependence on materials for thermoelectric performance, an overview of how to predict the performance of various materials and structures based on fundamental quantities is lacking. In this paper we present a review of the the oretical models that were developed since thermoelectricity was first observed in 1821 by Seebeck and how these models have guided experimental material search

for improved thermoelectric devices. A new quantum model is also presented, which provides opportunities for the optimization of nanoscale materials to enhance thermoelectric performance.

1.2 The Problem of Study

Research in recent years has been focused on developing both thermoelectric Structures and materials that have high efficiency

1.3 The Aim of Study

The aim of this work is to construct models that have guided experimental material search for improving thermoelectric devices and Also a new quantum model, which provides opportunities for the optimization of nanoscale materials to enhance thermoelectric performance.

1.4 Presentation of the thesis

This thesis consists of four chapters one is the introductions, in chapter two the thermoelectric and application is presented, Chapter three is concerned with Density of States, Fermi Energy and Energy Bands. In chapter four the practical work is exhibit.

Chapter Two

Thermoelectric Effects and Applications

2.0 Introduction:

Thermoelectric devices have gained importance in recent years as viable solutions for applications such as spot cooling of electronic components, remote power generation in space stations and satellites etc. These solid-state devices have long been known for their reliability rather than their efficiency; they contain no moving parts, and their performance relies primarily on material selection, which has not generated many excellent candidates. Research in recent years has been focused on developing both thermoelectric structures and materials that have high efficiency. In general, thermoelectric research is two-pronged with (1) experiments focused on finding new materials and structures with enhanced thermoelectric performance and (2) analytical models that predict thermoelectric behavior to enable better design and optimization of materials and structures. While numerous reviews have discussed the importance of and dependence on materials for thermoelectric performance, an overview of how to predict the performance of various materials and structures based on fundamental quantities is lacking. In this paper we present a review of the theoretical models that were developed since thermoelectricity was first observed in 1821 by Seebeck and how these models have guided experimental material search for improved thermoelectric devices. A new quantum model is also presented, which provides opportunities for the optimization of nanoscale materials to enhance thermoelectric performance.

2.1 Thermoelectric Properties

When two ends of a wire are held at different temperatures, a voltage develops across the two sides. This effect is known as the Seebeck effect, which was discovered by Seebeck in 1821 and published in 1822 [1]. The voltage between the two ends is proportional to the temperature difference across the wire provided the temperature gradient is small. The proportionality Constant is defined as the Seebeck coefficient or thermoelectric power and is obtained from the ratio of the voltage generated and the applied temperature difference.

$$s = \frac{\Delta V}{\Delta T}. \tag{2.1.1}$$

In 1834, the Peltier effect, a companion to the Seebeck effect, was discovered [2]. This effect occurs when a current passes through a wire. The current will carry thermal energy so that the temperature of one end of the wire decreases and the other increases. The Peltier coefficient $\pi_{12}$is defined as the heat emitted per unit time per unit current flow from conductor 1 to 2. Therefore, this heat is directly proportional to the current passing through the junction as described by Eq.(2.1.1).

$$dQ = \prod dI. \tag{2.1.2}$$

The Peltier effect is often overwhelmed by irreversible Joule heating, which also originates from electronic current. The Thomson effect was predicted in 1854 and found experimentally in1856 [3]. The Thomson effect occurs when a current flows across two points of a homogeneous wire having a temperature gradient along its length and heat is emitted or absorbed in addition to the Joule heat. The Thomson coefficient $\mu_T$is positive if heat is generated when positive currentflows from a higher temperature to lower temperature.

$$dQ = \mu_T \frac{\partial T}{\partial x} dx dI. \tag{2.1.3}$$

The three thermal–electrical properties provide the basis for modern direct energy conversion devices and their exploitation has been the subject of considerable research. In 1912,Altenkirch [4,5] introduced the concept of a figure of merit when he showed that good thermoelectric materials should possess large Seebeck coefficients, high electrical conductivity to minimize Joule heating and low thermal conductivity to retain heat at the junctions that will.

2.2 Development of Semiconductor Thermoelectric Materials

Initial thermoelectric materials studied were metals, which display Seebeck coefficients of a few tens of $\mu V/K$. However, in the middle of the 20th century, interest turnedtowards semiconductors as thermoelectric materials despite small ratios of electrical to thermalconductivity, due to their high Seebeck coefficients and heat conduction dominated by phonon transport. In 1952 Ioffe [7] studied the change in semiconductor thermal conductivity of a material relative to its position in the periodic table. He found that for larger mean atomic weight, the thermal conductivity was lower. This behavior was attributed to the increase in density that caused the velocity of sound in the crystal to decrease leading to a subsequent decrease in thermal conductivity. Since mobility of electrons serves as a direct relation between the crystal structure and electrical conductivity, Goldsmid [8] studied the ratio of mobility μ and thermal conductivity κ as a function of the mean atomic weight. Using the relationship proposed by Shockley and Bardeen [9] for mobility in semiconductors and Pierls relationship for thermal conductivity, he calculated the ratio as a function of the electron mean free path le and phonon mean free path l pin crystals.

$$\frac{\mu}{k} = \frac{4e\rho_m}{cv_s(2\pi m_e k_B T)^{1/2}} \frac{l_e}{l_p} \qquad (2.2.1)$$

Here$\rho_m$is the mass density; υ_s the velocity of sound and c is the septic heat of the crystal; and me use the electron mass and charge respectively. Using material properties measured for some common semiconductors they plotted the above ratio against the mean atomic weight of the semiconductors seen in Fig. (2.2.1). Applying the above mentioned selection rules of choosing materials with high Seebeck coefficients and high atomic weights led to the discovery of bismuth telluride (Bi2Te3) in 1954 by Goldsmid [10] that provided cooling of 26 ◦C. Bismuth telluride has a hexagonal structure with mixed ionic–covalent bonding along the lattice planes and the weak vander Waals bonding perpendicular to the planes. The hexagonal structure ensures high anisotropy in the lattice conductivity with a factor of 2 decrease in the thermal conductivity in the direction perpendicular to the planes. Bismuth telluride also has a multivalve bands structure with multiple anisotropic constant energy surfaces that have a small effective mass in one direction and large effective masses in the other two directions. Since smaller effective mass leads to high electron mobility, choosing the appropriate growth direction of bismuth telluride is necessary for good thermoelectric performance.

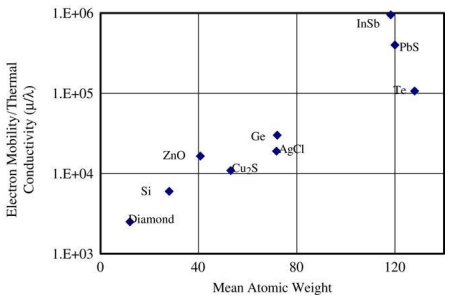

Fig (2.2.1). Ratio of Electron Mobility to Thermal Conductivity Of Thermoelectric Materials

In 1956, Ioffe et al. [11] suggested that alloying a semiconducting thermoelectric material with anisomorphous substance – materials having the same crystalline

structure – would enhance the figure of merit by reducing lattice thermal conductivity without affecting carrier mobility. They suggested that phonons would scatter due to the disturbances in the short-range order but the preservation of long-range order would prevent scattering of electrons and holes. This led to an extensive study of the thermoelectric performance of various semiconductor alloy systems over a wide range of temperatures.

Birkholz in 1958 [12] and Rosi in 1959 [13] showed that alloying $Bi_2Te_3$with Sb_2Te_3. OrBi_2Se_3greatly reduced the thermal conductivity. They also showed that adding even 5% ofSb_2Se_3greatly improved the figure of merit by raising the band gap that reduced am bipolar conduction i.e. contribution due to both electrons and holes to electrical conductivity and thermal conductivity. These studies led to the formation of a pseudo-ternary $Bi_2Te_3-Sb_2Te_3-Sb_2Se_3$system. The studies showed that the best n-type material was the Bi2Te3rich alloys while the bestp-type performance was obtained from the Sb2Te3pseudo-ternary alloys with an average figure of merit of 3.3×10−3K−1from both types at room temperature [14]. In general however, bismuth and bismuth telluride alloys are good thermoelectric materials only below room temperature. At room temperature and above, the relatively small band gap causes mixed conduction due to both electrons and holes leading to reduced Seebeck coefficient.

At temperatures above those that bismuth telluride can be used, materials like lead telluride are found to have very good thermoelectric properties in the range of 300–700 K. Lead telluride belongs to the lead chalcogenides system similar to materials such as PbS and PbSe. Leadchalcogenides have a cubic (NaCl) rock-salt structure with a FCC unit cell. They are polar semiconductors with a mixed ionic–covalent bond with the electrons traveling mainly in the caution (Pb) sub lattice and the holes in the anion chalcogenidesub lattice. Similar to bismuth telluride, lead

telluride (PbTe) has high mean atomic weight and a multi valley and structure. Having slightly higher band gap of 0.32 eV at 300 K, lead telluride produces higher Seebeck coefficients compared to bismuth telluride. While it has higher lattice thermal conductivity than bismuth telluride at room temperature, it eventually produces higher ZT values as the temperatures raised. Lead telluride also forms isomorphs solid solutions with lead selenide and tin telluride leading to lower thermal conductivities and improved ZT values. Rosi et al. [14] in 1961studied the band gap of the PbTe–SnTe system and determined that band reversal effect actually causes the band gap to go to zero at the composition Pb0.4Sn0.6Te and hence recommended that lower compositions of tin telluride would ensure sufficient band gaps leading to Z T values near 1 for n-type $PbTe-SnTe$ alloys at 700 K [15]. Another type of alloy system that gives Z T values around 1 for temperature range around 700 K are alloys between $AgSbTe2$ and $GeTe$ called TAGS [16]. These alloys possess the same rock-salt structure of $PbTe$ over partof the compositional range. When the composition of GeTe is greater than 70%, it transits to arhombohedral structure. The lattice strain associated with this phase transition is also believedto contribute to reduced lattice thermal conductivity values around 1.5 W/m K. At higher temperature ranges of 600–1300 K, silicon and germanium which are bad thermo electrics due to their high thermal conductivity at room temperature can be alloyed to obtain SiGe alloy, afar superior material for thermoelectric generation [17]. The large band gap of silicon makes silicon rich alloys such as $Si_{0.7}Ge_{0.3}$ suitable for high temperature applications since problems with minority carrier dominance do not arise. The large phonon scattering ensures low thermal conductivity without affecting the electron mobility making it possible to obtain ZT values of 0.5and higher [18].

Materials exhibit the highest possible thermal conductivity in the crystalline state and the lowest conductivity in the amorphous state. Based on this concept Slack in 1979 [19] proposed that the smallest possible lattice conductivity can be predicted by setting the mean free path of the phonons equal to that in the amorphous state. This observation prompted extensive research into materials that are termed as phonon glass and electron crystal (PGEC). These materials have very complex structures such as compounds of Borides (YB_{68}) [20], compounds of silver–thallium($TIAsSe_3$) [21] and H_2O. These materials contain groups of atoms or molecules that do not have precisely defined positions or orientations. The lack of long-range order causes the atoms or molecules to rattle and act as phonon scattering sites reducing the thermal conductivity to around 0.5 W/m K.

Another class of materials is called Skutterudites, which are complex materials with a chemical formula of ReTm4M12where Re is a rare earth element such as lanthanum or cerium,Tm is a transition metal such as cobalt, iron, etc. and M is a metalloid such as phosphor ,arsenic, or antimony. Binary skutterudites have the chemical formula of TmM_3, and its crystalstructure has the unique feature of containing two large empty spaces within each unit cell.While the binary structures have reasonably large Seebeck coefficients around 200 μV/K, they still exhibit very high thermal conductivities [15]. When a rare earth element is mixed with the binaryskutterudite, the heavy atom of the rare earth element occupies the empty space of the crystal [22]. In addition to causing large impurity scattering of phonons in these materials, the loosely bound heavy atoms rattle in their cages enhancing scattering of phonons and reducing thermal conductivity by an order of magnitude at room temperature. Skutterudites have been found to have a figure of merit greater than unity at temperatures around 700 K.

Additional examples of PGEC materials are inorganic catharses with the chemical formulaA8B46where B represents for example either gallium or germanium or a combination of the two elements [15]. Catharses consist of an open framework of gallium and germanium atoms that act as an electron crystal. Guest atoms are selectively incorporated in nano cavities in the crystal. The guest atoms vibrate independent of the crystal structure scattering phonons in the process. These materials are found to be very promising for thermoelectric applications at temperatures above 600oC. Catharses can be made of tin, silicon, antimony, etc. Examples of some good thermo electric catharses are $Sr_8Ga_{16}Ge_{30}$, Cs_8Sn_{44} as well as Zn_4Sb_3 that has been observed togive Z T values of 1.3 at 400 K. More recently an alloy of Pb–Sb–Ag–Te abbreviated as LAST was developed as n-type thermoelectric material having Z T values around 1.7 [23,24]. These alloys have nano-sized inclusions during synthesis that act as phonon scattering sites. A similar p-type alloy dubbed as SALT was observed to have Z T values around 1.6, the highest known for p-type thermoelectric materials.

Beyond the development of bulk materials with enhanced thermoelectric properties, superlatives have been proposed as structures that may improve Z T . These alternating layers of materials can be manufactured from alloys that are good thermoelectric materials to start with such as Bi_2Te_3/Sb_2Te_3, Bi_2Te_3/Bi_2Se_3as well as $PbSeTe/PbTe$ quantum dot superlattices,$Si/Si_{1-x}Ge_x$and Si/Gesuperlattices [25]. By adding interfacial scattering sites, the thermalconductivity of these structures can presumably be reduced. While fabrication of superlatticefilms and wires can take advantage of the advances made in semiconductor manufacturing technology such as lithography, electroplating, etc., significant challenges exist in translating the high Z T performance of bulk materials into similarly performing nanostructures. In this regard the biggest

bottleneck is the electrical conductivity which is dominated by contact resistance. The anisotropic nature of most nanoscale materials also makes their thermal conductivity performance unpredictable and difficult to measure. Measurement of thermoelectric propertieat the nanoscale is especially difficult as the substrate and buffer layers can overwhelm the Seebeck coefficient and electrical conductivity measurements. The challenges and high costs associated with nano scale measurements places special emphasis on the need to have a detailed understanding of electron–hole–phonon transport at the nano scale for a better prediction of thermoelectric performance. The models used to predict thermoelectric parameters must include the effect of various factors such as electron and phonon mean free paths, electron mobility, effect of band gap, substrate strain etc. Moreover, quantum confinement effects in low-dimensional structures, while increasing the density of states per unit volume at the Fermi level, can alsolead to reduced electrical conductivity due to the limited energy states available for electron transport. Similarly while phonon scattering and confinement at the super lattice interfaces can lead to reduced thermal conductivity, its impact on electron and hole transport through confinedcarrier-phonon scattering also has to be better understood. There has never been a greater need fora strong model that can couple both quantum and scattering effects to predict transport behavior innanoscale devices. In the next few sections, we present a review of the various models used to predict thermoelectric performance of bulk as well as low-dimensional structures with a view to identify and distinguish their ability to incorporate the necessary fundamental physics that guide thermoelectric behavior in materials.

2.3 Development of Modeling of Thermoelectric Coefficients

In 1928, Somerfield [26] put forth a comprehensive model on free-electron theory in metals using Fermi–Dirac statistics instead of Maxwell Ian statistics for the free-electron theory in metals developed by Lorentz. Somerfield assumed that only the valence electrons in a metal formed a free-electron gas that obeyed the Fermi–Dirac distribution f_0. Sommerfeld [27] studiedthermoelectric phenomena in metals where various combinations of the electric current and temperature gradient $\partial T / \partial x$ were applied on a wire. From his calculations he obtained equationsfor the electrical conductivity σ , thermal conductivity κ and Thomson coefficient μ_T. In allhis calculations Somerfield assumed conditions of local thermodynamic equilibrium and the number of electrons to be independent of temperature, and the mean free path of the electrons to be independent of their velocity ν.

$$\sigma = \frac{4\pi e^2}{3m_e}\left(\frac{m_e}{h}\right)^3 \int_0^\infty f_0 \frac{\partial}{\partial v}(l_e v^2) dv \tag{2.3.1}$$

$$k = \frac{4\pi m_e}{6}\left(\frac{m_e}{h}\right)^3 \left[\int_0^\infty l_e v^5 \frac{\partial f_0}{\partial x} - \frac{\int_0^\infty f_0 \frac{\partial}{\partial v}(l_e v^4) dv}{\int_0^\infty f_0 \frac{\partial}{\partial v}(l_e v^2) dv} \int_0^\infty l_e v^3 \frac{\partial f_0}{\partial x} dv\right] \tag{2.3.2}$$

$$\mu_T = \frac{2\pi^2 m_e k_B^2 T \lambda^2}{3eh^2} \tag{2.3.3}$$

Wherevers the electron mass, h is the Planck's constant and λ is the de Broglie Wave length me of electrons.

Bloch [28] solved the wave equation for periodic metallic lattice and showed that if the latticeis perfect, the electron would travel infinitely through it and only by taking into consideration the thermal motion of the lattice and the effect of impurities would finite conductivity be obtained. In addition, Bloch showed that the application of Pauli's exclusion principle eliminated the direct proportionality between the number of free electrons and the electrical conductivity. Conduction

under an applied field would then take place only if the final energy levels are unoccupied such that the electrons near the Fermi level can make transitions and take part in conduction. Bloch called these electrons conduction electrons. Based on these ideas Bloch introduced temperature dependence of electronic conduction in metals where the electric resistance varied directly with the absolute temperature for high temperatures and varies as $T^5$for low temperatures. Bloch'stheory of electrical conduction could not be easily extended to semiconductors as it seemed tosuggest that a lattice should have nearly infinite conductance at low temperatures while in realitythe conductivity of semiconductors is very low at low temperatures due to limited number of free electrons. It also could not explain the non-conductivity of insulators. In 1931, Wilson [29] extended Bloch's theory to semiconductors and developed a formal theory of electron transporting semiconductors and insulators with emphasis on the temperature dependence of electrical conductivity. Wilson's work was further extended to study Hall coefficients and thermoelectric power of semiconductors by Bronstein [30] in 1932 and Fowler [31] in 1933 but neither of the results by these authors were in a form suitable for comparison with direct experimental data or predictions of thermoelectric power from measured Hall and resistivity data.

In his book The Theory of Metals in 1953 Wilson [32] gave a comprehensive analysis of the conduction mechanism and thermoelectric performance of metals and semiconductors under the relaxation time approximation taking into account the effect of electron scattering with acoustic and optical phonons and electron–impurity scattering. Based on his calculations, the relaxation time in metals for electron–phonon scattering was calculated to be proportional to $\varepsilon^{3/2}T^{-1}$ whereε is the electron energy. This relation is the same result that was obtained by Bloch for metals. Inthe case of semi conductors the distribution of electrons is taken to

be$f_0 = \exp^{-(\varepsilon-\varepsilon_f/k_B T)}$ and restricting the phonon energy range to values around the Fermi energy ε_f , Wilson calculated theelectrical conductivity σ to be proportional to $n_e m_e^{*-5/2} T^{-3/2}$ where $m_e^*$is the effective massof the electron and $n_e$is the number of free electrons. By arriving at a direct proportionalitybetween the electrical conductivity and number of free electrons, Wilson was able to show thatsemiconductors have very low conductivity at low temperatures due to the very small number of free electrons available for conduction.

In 1953 Johnson and Lark-Horovitz [33] used Somerfield's model of electric current and thermal current to calculate thermoelectric coefficients for three different cases: (1) impurity temperature range where all the carriers are either n-type or p-type such that the concentration of carriers remains constant with temperature until intrinsic carrier effects become important; (2)transition temperature range where in addition to n- and p-type carriers, intrinsic carriers also exist and hence $n_e \neq n_h$; (3) intrinsic temperature range where intrinsic carrier dominates the electrons and holes from donors and acceptors such that $n_e = n_h$. The authors used Maxwellstatistics to describe the carrier distribution in the semiconductors. The mean free path was said to be affected by lattice vibrations where, similar to Somerfield, it was expressed to be independent of carrier energy. In the impurity and transition range an additional mean free path due to impurities was included where the mean free path was expressed as a function of carrier kinetic energy ε as $l_{imp} = aE_g\varepsilon^2$where a $E_g$is the temperature variation of the bandgapwidth and was found from the measured thermoelectric power curve of intrinsic germanium [33].The thermoelectric power for polycrystalline germanium having carrier concentrations ranging from $10^{15} - 7 \times 10^{18} cm^3$was calculated using these equations and compared to experimentsconducted by Lark-Horovitz, Middleton, Miller Scanlon and Walerstein [34] over a temperaturerange of 78–925

K. For impurity temperature range of approximately 78–300 K there was lot of scatter in the experimental data and the theoretical predictions were not in good agreement with the experiments. In the transition and intrinsic range of temperatures greater than 300 K there was good agreement between experiments and theory. Despite being founded on equilibrium principles, these models were important in establishing limits to the performance of bulk materials as will be shown later.

When Lord Kelvin (Thomson) [35] formulated his theory of thermoelectric phenomena in1854 he suggested that similar to the reciprocal relations between force and displacement in a mechanical system in equilibrium, there exist reciprocal relations between two or more irreversible transport processes that interfere with each other when they take place simultaneously in a thermodynamic system. Accordingly if J is the electric current due to an applied field and Q the thermal current due to the application of a temperature gradient, then for independent processes the electro-motive force that drives the electric current is given by

$$X_1 = R_1 J \tag{2.3.4}$$

WhereR_1 is the resistance to current flow and the force that drives the thermal current is given by

$$X_2 = R_2 Q \tag{2.3.5}$$

Where$R_2$is the resistance to the flow of thermal current. However since these two processesmutually interfere with each other, two forces X1and X2must be expressed as a combination of the two resistances $R_1$and R_2as

$$X_1 = R_{11} J + R_{12} Q \tag{2.3.6}$$

$$X_2 = R_{21}J + R_{22}Q \tag{2.3.7}$$

Thomson suggested that as long as there is no heat conduction from one part of the circuit to another, $R_{12} = R_{21}$. Thomson's reciprocal relations were examined by Onsager in 1931 [36]who calculated the thermoelectric properties as the entropy flow per particle due to (1) he at flow from high temperature to low temperature and (2) degradation of electrochemical potential energy into heat. From the macroscopic laws governing the thermoelectric process, the electric current J and the thermal current Q were expressed as

$$-J = L_{11}\frac{1}{T}\nabla\mu + L_{12}\nabla\frac{1}{T} \tag{2.3.8}$$

$$Q = L_{21}\frac{1}{T}\nabla\mu + L_{22}\nabla\frac{1}{T} \tag{2.3.9}$$

L_{11}, $L_{12}$and L_{22} are called kinetic coefficients are properties of the medium such aselectrical conductivity, thermal conductivity etc and in the absence of a magnetic field, Onsager stated that

$$L_{12} = L_{21} \tag{2.3.10}$$

Callen in 1948 [37] showed that while Onsager's relations strictly referred to specific transient irreversible processes, they could be extended to steady state processes by considering the system to be the limiting case of many small sections, each in local equilibrium. This assumption is incorporated by treating the temperature T and Fermi energy ε_f as functions of position. Callen pointed out that this assumption was similar to the assumptions made while using the Boltzmann transport equation where the system is assumed to be in local equilibrium by incorporating the deviation from the equilibrium term in the calculations. Here non-equilibrium effects were introduced to the problem.

In 1953 Frederikse [38] noticed large anomalies in the predicted vs. measured thermo electric power in germanium below temperatures of 200 K. They attributed these anomalies to the assumption of lattice thermal equilibrium commonly made when calculating thermo electric coefficients. The deviation from the equilibrium of the lattice at low temperatures results in a phonon current that interacts with the electron current. Frederikse modified Lark-Horovitz'smodel to include an additional term inversely proportional to temperature that would account for the deviation from equilibrium of the lattice at lower temperatures. Onsager's reciprocal relations were used by Price [39] in 1956 where he used a modification of the Johnson–Lark-Horvitz model [40] to calculate the thermoelectric coefficients in isotropic semiconductors. The thermo electric parameters were calculated phenol menologically as a function of the electron and hole conductivities using average values of the electric and thermal currents.

$$\sigma = \langle J \bullet J \rangle \tag{2.3.11}$$

$$S = \frac{1}{\sigma T} \langle J \bullet Q \rangle \tag{2.3.12}$$

$$\kappa_e = \frac{1}{T} \langle Q \bullet Q \rangle \tag{2.3.13}$$

The carrier energy was said to be affected by contributions from (1) electrostatic field (2) band edge energies (3) band gap and at low temperatures (4) entrainment of the lattice energy due to carrier–lattice collisions known as phonon-drag effect where phonons carrying a thermal current tend to drag the electrons with them from the hot side to the cold side [41]. The resulting expression for thermoelectric power was expressed in terms of the electron and hole electrical conductivities as

$$S = \frac{k_B}{2e\sigma} \left[\alpha(\sigma_e - \sigma_h) - \sigma_{\in} \ln\left(\frac{\sigma_e}{\sigma_h}\right) - \sigma_h \xi \right] \tag{2.3.14}$$

$$where\ \sigma = \sigma_e + \sigma_h \quad and\ \xi = \log\left(\frac{\mu_e}{\mu_h}\left(\frac{m_e}{m_h}\right)^{\frac{3}{2}}\right).$$

Price assumed that the electron and hole mobility's were independent of doping and used these vs. σ plot to graphically obtain the value of α, which represents the optimal performance, as shown in Eq. (2.3.14). Price showed that the graph (shown in Fig.(2.1) formed a loop where n-type materials are at the bottom of the loop and p-type materials at the top. The value where $\sigma_e = \sigma_h$

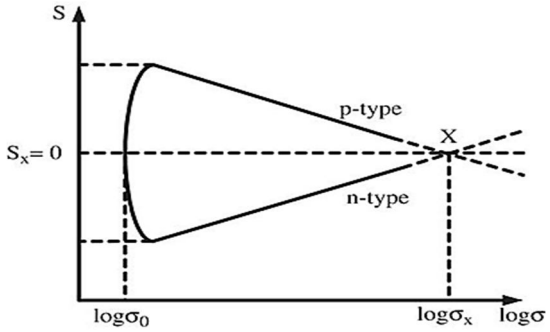

Fig. 2.3.1 Price's Doping Curve for Thermoelectric Power

corresponded to the minimum value of σ where minimum thermoelectric power is obtained due to bipolar transport. In addition to the thermoelectric loop, another notable contribution made by Price was the study of the change in thermoelectric power of semiconductors under shear strain. He showed that shear strain would change the activation energy of the impurity donor atom binding a carrier in a many-valley band by decoupling the orbitals associated with the different valleys leading to a shift in the band edge energies. Price recognized that this shift in the band edge energies of the donor atoms would appreciably change the thermoelectric power of semiconductors especially at very low temperatures.

$$\alpha = 2\log\left(\frac{2\sigma_X}{\sigma_0}\right) \ldots \alpha \gg 1. \qquad (2.3.15)$$

Ioffe in 1957 [6] gave a simple explanation to calculate the Seebeck coefficient based on thermodynamic considerations. Consider a junction of two conductors through which one coulomb of charge passes at an infintesimally slow rate such that the current is very small. The entire circuit is assumed to be at constant temperature T such that there is no heat conduction or joule heat loss allowing the system to be treated to be in equilibrium. Since the two conductors are in equilibrium their chemical potentials are equal such that $\varepsilon_{f_1} = \varepsilon_{f_2} = \varepsilon_f$. For a reversible,open system, the definition of internal energy can be written as

$$U_i = T_s + \varepsilon_f. \tag{2.3.16}$$

The average energy U as well as the entropy s of the electrons in the two conductors is different. Since the chemical potential of the two conductors is equal, we can write

$$U_i = T_s + \varepsilon_f. \tag{2.3.17}$$

When an electron passes through a junction of two conductors its average energy changes by $U_{i_1} - U_{i_2}$. This difference in electron energy is generated in the form of Peltier heat π_{1-2}at thejunction.

$$U_{i_1} - U_{i_2} = \pi_{1-2}. \tag{2.3.18}$$

The relation between Peltier heat and Seebeck coefficient is given by $ST = \pi_{1-2}$. From Eqs. (2.3.17) and (2.3.18) the Seebeck coefficient is obtained as

$$s = \frac{\pi_{1-2}}{T} = \frac{U_{i_1} - U_{i_2}}{T} = S_1 - S_2. \tag{2.3.19}$$

Eq. (2.3.19) describes the Seebeck coefficient as the flow of entropy per unit charge across a junction .From this definition and Eq. (2.3.20), the Seebeck coefficient across the junction can be written as

$$S = \frac{1}{e}\left(\frac{\bar{\varepsilon} - \varepsilon_f}{T}\right) \tag{2.3.20}$$

where ε is the average electron energy passing across the junction. If ε is the energy of each electron passing through the junction and $f(\varepsilon)$ is the distribution function of the electrons, theaverage electron energy across the junction is calculated as

$$\bar{\varepsilon} = \frac{\int_0^\infty \boldsymbol{\varepsilon f(\varepsilon) d\varepsilon}}{\int_0^\infty \boldsymbol{f(\varepsilon) d\varepsilon}}. \tag{2.3.21}$$

Using Fermi–Dirac statistics to describe electron distribution in near degenerate semi conductors and a constant relaxation time, power-law approximation to describe carrier energy dependent mean free path of the electrons,

$$\overline{\ell_e} \propto \varepsilon^r. \tag{2.3.22}$$

Ioffe calculated the Seebeck coefficient in a semiconductor as

$$s = \frac{k_B}{e}\left[\left(\frac{r+2}{r+1}\right)\frac{f_{r+1}\left(\frac{\varepsilon_f}{k_B T}\right)}{f_r\left(\frac{\varepsilon_f}{k_B T}\right)} - \frac{\varepsilon_f}{k_B T}\right]. \tag{2.3.23}$$

The Fermi integrals in Eq. (2.3.23) are calculated from

$$f_r\left(\varepsilon_f / k_B T\right) = \int_0^\infty \frac{x^r}{e^{(x - \varepsilon_f / k_B T)+1}} \tag{2.3.24}$$

Where$x = \varepsilon / k_B T$ is the reduced energy for electrons. Ioffe calculated the electrical conductivitythrough the relation $\sigma = n_e e\mu$, where $n_e$is the electron density given by Fermi–Dirac statistics as

$$n_e = \frac{4\pi(2m_e^* k_B T)^{3/2}}{h^3} f_{1/2}\left(\frac{\varepsilon_f}{k_B T}\right) \tag{2.3.25}$$

andμ is the temperature dependent mobility of the electrons. Temperature dependency ofmobility was included through the relation $\mu = \mu_0 k_B T^{r+1}$where μ_0 is the mobility at absolute 0 K. Thermal conductivity was calculated as a sum of the contributions from the electrons as well as lattice vibrations i.e. phonons. The lattice conductivity was obtained from

$$k_{ph} = \frac{1}{3} c v_s l_p \tag{2.3.26}$$

c is the specific heat obtained from the Debye model, v_s is the sound velocity and $l_p$is thephonon mean free path. The electron contribution to thermal conductivity calculated from thegeneral case of the Wiedemann–Franz law is given by

$$\frac{k_{el}}{\sigma} = A\left(\frac{k_B}{e}\right)^2 T \tag{2.3.27}$$

The coefficient A accounts for the various scattering mechanisms and is equal to

$$A = \left[\frac{r+3}{r+1}\frac{f_{r+2}\left(\frac{\varepsilon_f}{k_B T}\right)}{f_r\left(\frac{\varepsilon_f}{k_B T}\right)} - \frac{(r+2)^2}{(r+1)^2}\frac{f_{r+1}^2\left(\frac{\varepsilon_f}{k_B T}\right)}{f_r^2\left(\frac{\varepsilon_f}{k_B T}\right)}\right] \tag{2.3.28}$$

where the scattering parameter $r$changes depending on the type of scattering. For example,the value of r is -1 for scattering with optical phonons while for ionized-impurity scattering,which is predominant in metals, the value of r is determined to be equal to be 2. This model combines transport concepts with fundamental properties to achieve a reliable estimator of the thermoelectric properties of bulk materials.

In 1959 Chasmar and Stratton [42] used Ioffe's model to calculate the optimum value of the Fermi level that would give the maximum value of$Z\,T$ for various values of the scattering parameter . Using classical statistics and Fermi–Dirac

statistics respectively they obtained the maximum value of $Z\,T$ as a function of material parameters. They introduced a material parameter βwhich was a function of the effective mass and temperature of the system and thelow carrier concentration mobility μ.

$$\beta = \frac{\frac{2e(2\pi m^* k_B T)^{\frac{3}{2}}}{h^3}\left(\frac{k_B}{e}\right)^2 T\mu}{k_l}. \qquad (2.3.29)$$

For a given temperature and material parameter β, the optimum value of Fermi energy to maximize $Z\,T$ was calculated for various scattering parameters r. Their calculations indicated that the value of β and hence the figure of merit Z T must increase as the temperature rises. More importantly their work was the first to identify the impact of band gap on the figure of merit. While materials with large band gaps were found to have low carrier mobility and high thermal conductivity, small band gap materials would result in low Z T values at high temperatures due to increased minority carrier contribution to thermal conductivity. In addition ionic compounds were shown to be poor thermoelectric materials due to very high polar scattering of electrons, which decreases mobility. Chasmar and Stratton combined their analysis with the results of Golds mid [8] whose studies on the ratio of mobility to thermal conductivity as a function of the atomic weight led to the discovery of bismuth telluride. From their analysis semiconductors with optimal values of β between 0.1 and 0.2 and high atomic weight include sulphides, selenides and telluride's of heavy metals such as lead or bismuth. Though these compounds have low band gap at0 K ($\leq 0.22\,eV$), the bandgap increases with temperature. Cadmium telluride on the other handhas a large bandgap, 1.45 eV at 300 K but the material parameter β is only 0.03–0.06. Basedon the above studies Chasmar and Stratton proposed that a combination of cadmium telluride orselenide

(large bandgap, small β) with a telluride or selenide of small bandgap and large β would result in a good thermoelectric material.

Attempts to find an upper bound to the figure of merit were made by various researchers. Littman and Davidson [43] used irreversible thermodynamics to show that no upper limit was imposed on Z T by the second law. However, Rittner and Neumark [44] showed that it was important to employ a combination of statistical or kinetic methods with a proper physical model of semiconductors to study the figure of merit. Simon [45] studied the optimum Z T value in two band semiconductors as a function the minimum band gap Eg, material parameter β for electrons and holes and the scattering parameter r for electrons and holes. He defined a parameter$\gamma = (m_e/m_h)^{3/4}(\mu_e/\mu_h)^{1/2}$that he varied by adjusting the material parameters βe and βh. Whilehe could not arrive at a definite upper limit to the value of Z T his theoretical studies of optimumZT vs. $\gamma$for $Eg = 0$showed that very high values of Z T could be achieved in very smallbandgap semiconductors by doping. At this point, most of the fundamental physics required to fully describe thermoelectric performance was known. Yet, most transport models were still not sophisticated enough to simultaneously include all the pertinent physics. Significant progress was made in the fifties and the sixties towards analytically calculating the scattering parameters used in the Boltzmann transport equation. The most common modes of scattering included in the BTE were acoustic-phonon scattering through the deformation potential put forth by Bardeen and Shockley [6] and the polar-optical mode scattering put forth by Callen in 1949 [46] and Froehlich in 1954 [47]. In the case of elastic scattering such as acoustic-phonon scattering and ionized-impurity scattering, the relaxation time approach that characterizes the rate at which momentum decays can be used to solve the BTE. However in the case of inelastic scattering no relaxation time exists

and hence other methods to solve the BTE were developed such as the vibrational calculations approach put forth by Kohler in 1948 [48],the iteration method by Rode in 1970 [49] and the matrix method by Kranzer in 1971 [50].Meanwhile Kane in 1957 [51] determined accurately the structure of the lowest (000) conduction band minima at the center of the Brillouin zone as well as the wave functions in that valley. Using Kane's model of the band structure and electron wave functions, Rode [49] calculated the electron mobility in intrinsic, direct gap, polar, non-degenerate semiconductors using Maxwellian statistics. He included the three scattering mechanisms i.e. acoustic deformation potential scattering, polar optical-phonon scattering and piezoelectric scattering which heidentified as the most important mode of scattering for lower lattice temperatures such as for e.g. below 60 K in GaAs. The electron distribution function under the influence of a small electric field is described as a linear finite-difference equation, which was solved using a numerical iteration method. The mobilities resulting from using parabolic vs. non-parabolic bands described by Kane were compared. Non-parabolicity affected the calculated mobility by only 10% in wide band gap material such as GaAs while small band gap material such as In Sb showed a 50% decrease in the calculated mobility when non-parabolicity was in cluded .Good match between the predicted and measured mobility data was seen for GaAs between the temperature ranges of 150–400 K. While the poor match with measured data at high temperatures could not be explained, the results below 150 K were attributed to the non-inclusion of impurity scattering in the model which becomes prominent at low temperatures. In 1971 Rode [52]extended the previous study to calculate mobility and thermoelectric power in degenerate direct-gap, polar semiconductors using Fermi–Dirac statistics. In addition to piezoelectric scattering, longitudinal acoustic-phonon scattering and polar optical-phonon scattering, ionized-impurity scattering and heavy hole scattering were also

included in the calculations. Thermoelectric power was calculated from the short-current calculated from the perturbation distribution where the elides set equal to zero.

$$S = -\frac{\left(\frac{1}{e}\nabla\varepsilon_f + \frac{J}{\sigma}\right)}{\nabla T} \qquad (2.3.30)$$

Mobility and thermoelectric power were compared with experimental data for intrinsic In Sb, In As and In P. There was good agreement with measured mobility data for all three semiconductors above room temperature while below room temperature the mobility showed two orders of magnitude decrease compared to experiments. Electron–hole scattering was prominent above room temperature, polar mode inelastic scattering dominated at room temperature while impurity scattering was dominant below room temperature. Below 60 K in In Sb and 80 Kin In As, deformation potential acoustic mode scattering and piezoelectric scattering dominate electron mobility. Good agreement with experimental data was also seen in the case of thermoelectric power for various electron concentration levels at room temperature. However, for higher temperatures, the thermoelectric power showed slight deviation from experiments where multivalve conduction was suspected to dominate electron transport. Mahan in 1994 [53] extended Rode's work to study the optimum band gap in direct band gap semiconductors. Non-parabolicity was included using the two-band Kane model and the solution to the BTE was obtained using Rode's iteration method in the Gauss–Siebel formulation because inelastic scattering was included. Comparisons were made between Z T values for parabolic bands and non-parabolic bands with either elastic ionized-impurity scattering or inelastic polar optical-phonon scattering. They found that the dependence of Z T on the ban dag fell into two regimes. For Eg<6kB T the value of Z T decreased with decreasing band gap due to the increasing presence of

minority carriers. For $E_g > 10k_BT$ the value of ZT either increased or decreased depending upon the type of scattering involved. Additionally they found that the most important effect of non-parabolicity was to modify the effective mass values that in turn changed the value of the material parameter $\beta_0$present in the expression for ZT similar to the parameter β in Chasmar and Stratton's model. Mahan determined that in order to obtain higher values the value of β0 needs to increase implying that materials with higher effective masses or reduced thermal conductivity κ needed to be researched. Table 1 summarizes the progression

of thermoelectricity and the various models used for predicting thermoelectric performance since the first thermoelectric effect was discovered in 1821.

2.4 Development of Low-Dimensional Models for Thermoelectric Applications

The concept of mono crystalline semiconductor structures having a periodic potential in one dimension was proposed by Esaki and Tzu in 1970 [54] who called these structures super lattices .While several low-dimensional structures can be envisaged to improve thermo electric performance, super lattices provide a fertile conceptual tested and have been the focus of many studies. Esaki and Tzu suggested that the periodic potential could be obtained by periodic variation of alloy composition or variation of impurity density during epitaxial growth out of materials such as Si, Ge and their alloys, III–V, II–VI, compounds and their alloys etc. The dispersion relation in the direction parallel to the super lattice planes was assumed to be parabolicwhile in the cross-plane direction they used a sinusoidal approximation in the form of Mathieu'sequation [55]

$$E\left(k_{||}, k_{\perp}\right) = \frac{\hbar^2 {k_{||}}^2}{2m_e^*} + t(1 - \cos(k_{\perp} d)) \qquad (2.4.1)$$

Where is the super lattice period, $k_{\perp}$corresponds to the wave vectors in the cross-planedirection and kkcorresponds to the wave vectors in the in-plane direction of

the superlattices.The amplitude of the superlattice periodic potential is given by t. The authors found that under moderate electric fields in the cross-plane direction the confined energy bands and wave vector zones would result in a negative conductance that could lead to new ultra-high frequency oscillators. The negative conductivity will arise from the fact that electrons traveling perpendicular to the super lattice would experience negative effective mass beyond the inflection point in the sinusoidal E vs. k dispersion relation. In 1984 Friedman [56] suggested that the low-temperature ($k_BT < \varepsilon_f$) thermoelectric power S of a superlattice as a function of dopant concentration can be used to provide information about the one-electron density of states and the location and width of the mini-bands. Following Wilson's model for calculating thermoelectric power using Fermi–Dirac statistics in the BTE and assuming energy-independent momentum scattering rates, they showed mathematically that the thermoelectric power tends to diverge at the mini-band extreme. The divergence in S is smoothed out for energies greater than $k_BT$butthey were still discernible for low temperatures. In addition, anisotropy in the thermoelectric power was predicted for in-plane vs. cross-plane temperature gradient. For the next couple of years the low-temperature thermoelectric power of super lattices was predominantly used as atoll to understand the electronic structure and transport properties of super lattices [57,58] as well as the scattering dynamics of electrons and phonons in solids [59,60].In 1992, Mensah and Kanga [61] used the relaxation time approximation (RTA) model of the BTE with the sinusoidal dispersion relation for the confined direction of super lattices to obtain analytical expressions for the Seebeck coefficient and thermal conductivity of super lattices along the super lattice cross-plane direction. Defining 2Δ as the width of the lowest energy mini-band in the E vs. k regime, the thermo power and thermal conductivity are calculated for two ranges ofΔ. For $\Delta \ll K_BT$, the electrons in the superlattice are said to behave as a 2D electron gas whilefor$\Delta \gg k_BT$the electrons behave as a

3D gas. They suggested that by an optimal selection of Δ and d, the super lattice period, it is possible to obtain good-quality and efficient thermo elements. In 1993, and Hicks [62] proposed that layering highly anisotropic thermoelectric materials such as Bi2Te3alloys in the form of super lattices would make it possible to increase the figure of merit provided that the super lattice multilayers are made in a particular orientation. The model of the super lattice proposed by the authors involved layers of thin films with no barrier layers such that confinement effects originated only due to electron confinement in the thin films. They theorized that in addition to confinement effects that cause electrons to behave as a 2D gas, the layering would reduce thermal conductivity through phonon scattering and thus increase Z T. The layers were assumed to be parallel to the $x-y$ plane where they have a parabolic dispersionand a confined dispersion in the z direction as shown in Eq. (35) which unlike the sinusoidal dispersion used in the previous papers, treats the lowest sub band in the well to be flat similar to electrons confined in an infinite potential well.

$$\varepsilon\left(k_x, k_y\right) = \frac{\hbar^2 k_x^2}{2m_x^*} + \frac{\hbar^2 k_y^2}{2m_y^*} + \frac{\hbar^2 \pi^2}{2m_z^* a^2} \tag{2.4.2}$$

Using the dispersion relation and the equations for S, σ andk_{el} and k_{ph}specified by Ritter [44]they calculated the figure of merit $ZT$for transport along the x-axis in terms of the Fermi functions of order 1 and 0 (refer Eq. (2.4.1)) as well as the reduced Fermi energy ε∗ fand a material parameter B described in Eq. (2.4.2).

$$Z_{2D}T = \frac{\left(\frac{2F_1}{F_0} - \varepsilon_f^*\right) F_0}{\frac{1}{B} + 3F_2 - \frac{4F_1^2}{F_0}} \tag{2.4.3}$$

Where

$$\varepsilon_f^* = \frac{\left(\varepsilon_f - \frac{\hbar\pi^2}{2m_z^* a^2}\right)}{k_B T} \; and \;\; B = \frac{1}{2\pi a}\left(\frac{2k_B T}{\hbar^2}\right)(m_x m_y)^{\frac{1}{2}} \frac{k_B^2 T \mu_x}{e k_{ph}} \qquad (2.4.4)$$

The authors analyzed that the value of$Z_{2D}T$can be increased by using narrower layersthat will ensure increased phonon scattering and by choosing optimum current direction and layer orientation to maximize mobility. The $Z_{2D}T$values for Bi_2Te_3were predicted for two orientations of the multilayers, the x–y planes and the x–z planes. The results predicted an increase in Z T by a factor of 13 over the bulk value in the x–z plane for current flow along the x-axis for layers that are 3.8Δ thick. In the case of the x– y plane results predicted an increase in Z T by a factor of 3 over the bulk value for layers that are 10Δ thick. The dispersion model used in the above paper treats the quantum wells as decoupled such that there is no tunneling between the wells.

So fo and Mahan [63] analyzed the Z T predictions of a super lattice put forth by Hicks and Dresselhaus by incorporating alternating barrier layers having finite thermal conductivity in the super lattice and introduced a tunneling probability between the quantum wells in their calculations. They argued that quantum mixing between the wells due to tunneling leads to a broadening of the density of states from 2D to 3D. In addition, the finite thermal conductivity of the barrier region produces a parasitic effect of backflow of heat that would hinder the pumping of heat in the well. The authors used the RTA model to include electron density dependence on the electrical conductivity through the expression given by Drudge [29].

$$\sigma = n_e(e^2\tau/m_x). \qquad (2.4.5)$$

The dependence of the electrical conductivity on electron density ensures that if the well width a and chemical potential ε f are kept constant, just by increasing

the barrier width b, the electron density will decrease due to reduced tunneling probability causing the electrical conductivity to decrease and decrease Z T . Alternately, for a fixed barrier width, as the well width is reduced, the 2D density of states increases and proportionately increases the electrical conductivity as well as ZT. The thermal conductivity equation was also modified to include heat backflow at the barriers in the thermal conductivity. In addition they changed the value of B to be inversely proportional to the super lattice period d and not the well thickness a. Sofa and Mahan used their model to predict the ZT vs. well width values forBi_2Te_3layers in the x– y plane with transport along the x-axis. Using average values in the literature for the mobility μx and thermal conductivity κ, they found that there was improvement in ZT due to the enhancement of density of states at the bottom of the lowest sub band with decreasing well width but the amount of increase was not as high as originally predicted by Dresselhaus and Hicks. The change in Z T with decreasing well width was studied as a function of the barrier width. In all cases except for a 20Δ wide barrier the Z T values increase with decreasing well thickness. The decrease in Z T for the 20Δ barrier was attributed to tunneling through the barrier that causes quantum coupling between the wells leading to broadening of density of states making the 2D density of states to become 3D density of states and reduce Z T . The authors also point out that the flat sub band assumption works well when the Fermi level lies above the sub and at a distance greater than the value of kBT as electrons above and below the Fermi level have opposite contribution to the thermo power. Similar studies on the effect of tunneling and finite thermal conductivity contribution of the barrier material were done by Brodie and Reinbeck [64] in 1995 who studied the effects of confinement on the figure of merit of Bi2Te3superlattices using Kraig–Penny type sub band energy dispersion in the RTA model. They too found that the value of Z T2Dincreased as the well width decreased until tunneling between wells caused the

value of Z T2Dto reduce for further decrease in well width. In 2001 Brodie and Reinbeck [65] extended the BTE model with Kronig–Penny sub-bands to calculate thermoelectric coefficients in quantum well and quantum wire super lattices. The thermoelectric coefficients were calculated for the occupied sub-bands in each conduction band valley neglecting inter-valley scattering. The results for each valley were summed over all the multiple ellipsoidal conduction band valleys to obtain the overall thermoelectric coefficients. Elastic acoustic-phonon scattering through the deformation potential scattering and inelastic optical- phonon scattering using the solution to the inelastic 3D Boltzmann transport equation were in- clouded in the calculations. Optical phonons were assumed to be dispersion less with the dominant phonon energy to be the value of its zone center $\bar{}\omega 0$. The BTE solution for inelastic scattering was obtained by using an extension of Ritz's iterative method [66]. The thermoelectric coefficients were compared to the results of the constant relaxation time approximation (CRTA) and bulk values as a function of decreasing well width. In general, solutions based on the CRTA were found to predict much higher values for mobility compared to the inelastic solution. Power factor predictions made by both CRTA and inelastic scattering methods predicted lower values than the bulk which were attributed to electron confinement in the wells leading to reduced conductivity. The power factor values increased with decreasing well width due to increase in the 2D density of states and eventually matched the bulk power factor. However, further decrease led to electron tunneling that changed the 2D density of states to 3D lowering the power factor. These effects as seen previously were not captured by the CRTA model. The effect of scattering and band structure on the thermoelectric performance was demonstrated through the power factor studies done on two materials, PbTe and GaAs. PbTe has an anisotropic multi valley band structure while a single isotropic conduction band valley. At room temperature both acoustic-phonon and optical-

phonon scattering dominate in PbTe while only optical-phonon scattering dominates in GaAs. Accordingly the full solution of the BTE including elastic acoustic-phonon and inelastic optical-phonon scattering showed an increase of only a factor of two in the power factor of to its bulk value while GaAs showed a factor of 9.5 increase in its power factor. The ability to incorporate the full band structure information to calculate the thermoelectric coefficients was demonstrated by Sofa et al. in 2003 [67] when they presented a method of calculating the electronic structure from first principle calculations, which they included in the relaxation time approximation to calculate the transport coefficients. They defined a kernel of all transport coefficients known as the transport distribution that contains all the electro misinformation needed to obtain the thermoelectric coefficients directly for any given material as shown in Eq. (2.4.6).

$$S = \frac{ek_B}{\sigma}\int d\varepsilon\left(-\frac{\partial f_0}{\partial \varepsilon}\right)\Xi(\varepsilon)\frac{\varepsilon-\mu}{k_BT} \quad where\ \Xi = \sum_{\vec{k}} \vec{v}_{\vec{k}}\,\vec{v}_{\vec{k}}\vec{v}_{\vec{k}}. \qquad (2.4.6)$$

The group velocity values are obtained using the linear augmented plane wave (LAPW) method while the relaxation times are calculated for various scattering mechanisms using parameters found in the literature. Doping was included by changing the relative position of the Fermi level under the assumption that the ban structure remains unchanged as the Fermi level changes. The above method was used to calculate the thermoelectric coefficients for Bi2Te3 using experimentally determined thermal conductivity values for the various planes. The Seebeck coefficient for all doping levels was calculated using a constant relaxation time that gave the best fit with experimental data in the intrinsic region. For all doping levels, the Seebeck coefficient of the n-type material showed a better fit with experiments compared to the p-type. The model also captured effectively the anisotropy in the electrical conductivity of Bi_2Te_3 where the conductivity along

the basal plane can be four times greater than the conductivity along the trigon axis. The predictions for the figure of merit however did not show very good match with experiments with results for the n-type matching better than those for the p-type. Similar match with experimental data was obtained by Lee and Allman in 2006 [68] who calculated the thermoelectric coefficients using a tight-binding model with $sp^3d^5s^*$orbitals, nearest neighbor interactions and spin–orbit coupling for Bi2Te3 in the constant relaxation time approximation model. Table 2 summarizes the progression of models used for predicting thermoelectric performance in low-dimensional structures.

2.5 Nanostructured Thermoelectric Materials

The advent of quantum well nan of lm and nanowire super lattice structures that improve the value of ZT due to a number of advantages has shifted the focus towards understanding carrier transport behavior in nanostructures. Quantum confinement in nanostructures increases the local carrier density of states per unit volume near the Fermi energy increasing the Seebeck coefficient [62] while the thermal conductivity can be decreased due to phonon confinement [69,70] and phonon scattering at the material interfaces in the super lattices [62,71,72]. Normally, the electrical conductivity is assumed not to be significantly affected due to the large semiconductor band gap and the disparity between the electron and phonon mean free paths [25,73]. This assumption is also a consequence of the predominantly particle-based models. The combined benefits of reduced thermal conductivity and improved Seebeck coefficient imply a theoretically higher ZT compared to the bulk structures. However, experimental observations have not been able to achieve the presumed benefits of super lattice thermoelectric devices despite theoretically predicted improvements in ZT and experimentally observed

reduction in the thermal conductivity of super lattices compared to their bulk counterparts [74,75]. Hence there is a need to better understand the effect of all the significant factors contributing to the thermoelectric figure of merit of nan scale devices. In this regard, the two main phenomena that affect electron transport in nanostructures are (1) electron confinement and (2) electron scattering effects such as electron–phonon scattering, electron–impurity scattering etc. Shrinking device dimensions presents an increasing need for a quantum transport model that can effectively couple scattering effects. The need to incorporate scattering stems from the fact that while electron–phonon scattering usually helps restore thermodynamic equilibrium, shrinking device dimensions may not ensure enough scattering to restore equilibrium. The simultaneous consideration of scattering effects, which is usually described as particle behavior, and quantum effects, which are wave in nature, is confounding and computationally intensive. In this regard the non-equilibrium Green's function formalism provides a framework for coupling quantum effects and thermal effects to model electron transport in thermoelectric devices. Open boundary conditions allow the source and drain contacts to be coupled to the device through simple self-energy terms. In addition, the NEGF formalism does not require a statistical distribution of carriers within the device thus allowing for the rigorous incorporation of both elastic and inelastic scattering effects using the concept of Battier probes [76]. A brief synopsis of the formalism is presented here while a more thorough and detailed development can be found in [76] and [77]. The first reported use of NEGF to predict thermoelectric performance is found in [78–80]. True quantum simulations have to see widespread use, but modern devices demand this level of modeling.

Chapter Three

Density of States, Fermi Energy and Energy Bands

3.1 Introduction

This chapter is concerned with studying the density of states of beside Fermi energy and energy bands theory.

3.2 Density of states

3.2.1 Current and Energy Transport

The electric field E is interfered with two processes which are the electric current density j and the temperature gradient∇T . The coefficients come from the Ohm's law and the Seebeck effect.The field can be written as

$$E = \frac{j}{\sigma} \alpha \nabla T \qquad (3.2.1)$$

Where σ is the electrical conductivity and is the Seebeck coefficient. The heat flux (thermal current density) q is also interfered with both the electric field E and the temperature gradient ∇T . However, the coefficients are not readily attainable.

Thomson in 1854 arrived at the relationship assuming that thermoelectric phenomena and thermal conduction are independent. Later, Onsager [1] supported that relationship by presenting the reciprocal principle which was experimentally verified. The heat flux can be written as

$$q = \alpha T_j - k\nabla T \tag{3.2.2}$$

where k is the thermal conductivity consisting of the electronic and lattice (or phonon)contributions to the thermal conductivity as

$$k = k_e + k_l \tag{3.2.3}$$

In this chapter, only the electronic contribution to the total thermal conductivity is used.

$$q_e = \alpha T_j - k_e\nabla T \tag{3.2.4}$$

We consider a one-dimensional analysis in this chapter because most thermoelectric devicesreasonably holds one-dimension, so that tensor notations are

3.2.2 Electron Density of States

Dispersion Relation

From Equation (10.16) (combining the Bohr model and the de Broglie wave), we have

$$\lambda = \frac{h}{p} \tag{3.3.1}$$

This λ is known as the de Broglie wavelength. Using the definition of wave vector $k = 2\pi/\lambda$, we have

$$k = \frac{p}{\hbar} \tag{3.3.2}$$

Knowing the momentum p = mv, the possible energy states of a free electron is obtained

$$E = \frac{1}{2}mv^2 = \frac{p^2}{2m} = \frac{\hbar^2 k^2}{2m} \tag{3.3.3}$$

which λ is called the dispersion relation (energy or frequency-wave vector relation).

Effective Mass

In reality, an electron in a crystal experiences complex forces from the ionized atoms. We imagine that the atoms in the linear chain form the electrical periodic potential. If the free electron mass **m** is replaced by the effective mass m*, we can treat the motion of electrons in the conduction band as free electrons. An exact defined value of the wave vector k, however, implies complete uncertainty about the electron's position in real space. Mathematically, localization can be described by expressing the state of the electron as a wave packet, in other words, a group velocity. The group velocity of electrons in Figure 11.1 is the slope of the dispersion relation.

$$v_g = \frac{\partial \omega}{\partial k} \tag{3.3.4}$$

Since the wavelength is twice the lattice constant a, the boundaries at the zone in k-space is $k = \pm\pi/a$. The frequencyω associated with a wave vector of energy E is

$$E = \omega\hbar \quad \text{and} \quad k = \frac{p}{\hbar} \tag{3.3.5}$$

Where the two equations are known as the Planck-Einstein relations.

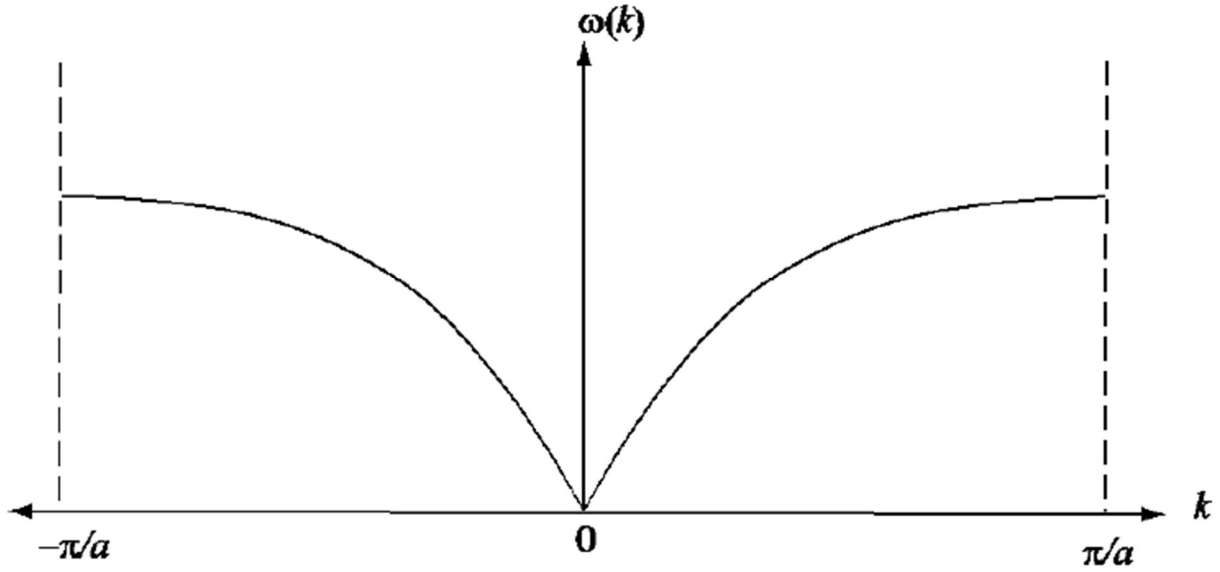

Figure (3.2.1) Dispersion Relation of A Group of Electrons with A Nearest Neighbor Interaction.

Notethatω is linear the boundaries of the Brillouin zone (k = ±π/a)for small k, and that $\frac{\partial \omega}{\partial k}$ vanishes at

$$v_g = \frac{1}{\hbar}\frac{\partial E}{\partial k} \tag{3.3.6}$$

The derivative of Equation (3.3.6) with respect to time is

$$\frac{\partial v_g}{\partial t} = \frac{1}{\hbar}\frac{\partial^2 E}{\partial k\,\partial t} = \frac{1}{\hbar}\frac{\partial^2 E}{\partial k}\frac{\partial k}{\partial t} \tag{3.3.7}$$

From Equation (3.3.5), we have $mv_g = \hbar k$ and $m\,\partial v_g/\partial t = \hbar\,\partial k/\partial t$. The force acting on the groupof electrons is then

$$F = m\frac{\partial v_g}{\partial t} = n\frac{\partial k}{\partial t} \tag{3.3.8}$$

Combining Equations (3.3.7) and (3.3.8) yields

$$F = \frac{\hbar^2}{\partial^2 E/\partial k^2}\frac{\partial k}{\partial t} \tag{3.3.9}$$

This indicates that there is an effective mass m*, which will replace the electron mass m.

$$\frac{1}{m^*} = \frac{1}{\hbar}\frac{\partial^2 E}{\partial k^2} \tag{3.3.10}$$

The effective mass m* is the second order of derivative of energy with respect to wave vector, which is representative of the local curvature of the dispersion relation in three dimensional space. The effective mass is a tensor and may be obtained experimentally or numerically.

3.4 Density of States

Thermoelectric materials typically exhibit the directional behavior. Therefore, in general we have

$$E = \frac{\hbar^2}{2}\left[\frac{k_x^2}{m_x} + \frac{k_y^2}{m_y} + \frac{k_z^2}{m_z}\right] \tag{3.4.1}$$

where mx, my, and mz are the principal effective masses in the x-, y-, z directions and here k is the magnitude of the wave vector.

$$k^2 = k_x^2 + k_y^2 + k_z^2 \tag{3.4.2}$$

This represents the surface of a sphere with radius k in k-space. We introduce a new wave vectors k' and an effective mass m' as

$$E = \frac{\hbar^2 k'^2}{2m'} \tag{3.4.3}$$

Equating Equations (3.4.1) and (3.4.3), we have a relationship between the original wave vector and the new wavevector as

$$k_x = \sqrt{\frac{m_x}{m'}}k'_x, k_y = \sqrt{\frac{m_y}{m'}}k'_y \text{ and } k_z = \sqrt{\frac{m_z}{m'}}k'_z \tag{3.4.4}$$

In Figure 11.2, we have the volume of a thin shell of radius k and thickness dk.

$$dk = dk_x dk_y dk_z = \sqrt{\frac{m_x m_y m_z}{m'^3}}dk'_x dk'_y dk'_z = \sqrt{\frac{m_x m_y m_z}{m'^3}}4\pi k'^2 dk' \tag{3.4.5}$$

The volume of the smallest wave vector in a crystal of volume L3 is (2π/L)3 since L is the largest wavelength. The number of states between k and k + dk in three-dimensional space is then obtained (see Figure 3.3.1)

$$N(k)dk = \frac{2.4\pi k'^2}{\left[\frac{2\pi}{L}\right]^3} \tag{3.4.6}$$

where the factor of 2 accounts for the electron spin (Pauli Exclusion Principle). Now the density of states g(k) is obtained by dividing the number of states N by the volume of the crystal L3.

$$g(k)dk = \frac{k'^2}{\pi^2}\sqrt{\frac{m_x m_y m_z}{m'^3}}dk' \tag{3.4.7}$$

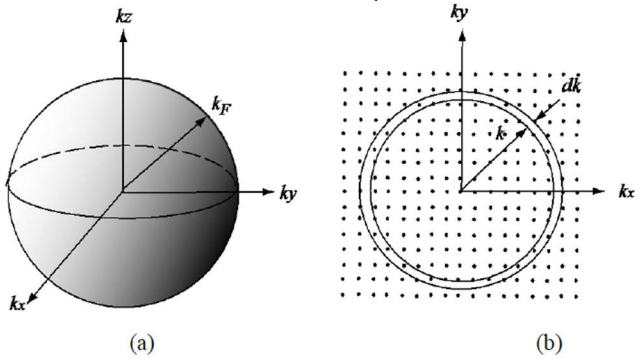

Figure (3.4.1) A Constant Energy Surface In K-Space: (A) Three-Dimensional View, (B) Lattice Points For A Two-Dimensional View. Spherical Band In

From Equation (3.4.3), we have

$$k' = \frac{\sqrt{2m'}}{\hbar}E^{1/2} \tag{3.4.8}$$

Differentiating this gives

$$\frac{\partial k'}{\partial E} = \frac{\sqrt{2m'}}{\hbar}E^{1/2} \tag{3.4.9}$$

Replacing this into Equation (3.4.7), m' is eliminated. The density of states per valley is finally obtained as

$$g(E) = \frac{1}{2\pi^2}\left[\frac{2m_d^*}{\hbar^2}\right]^{\frac{3}{2}} E^{\frac{1}{2}} \qquad (3.4.10)$$

where

$$m_d^* = \left(m_x m_y m_z\right)^{\frac{1}{3}} \qquad (3.4.11)$$

which is called the density-of-states effective mass, and mx, my, and mz are the principal effective masses in the x-, y-, z-directions. Most actual band structures for semiconductors have ellipsoidal energy surfaces which require longitudinal and transverse effective masses in place of the three principal effective masses (Figure 3.4.2). Therefore, the density-of-states effective mass is expressed as

$$m_d^* = \left(m_l m_l^2\right)^{\frac{1}{3}} \qquad (3.4.12)$$

where l m is the longitudinal effective mass and t m is the transverse effective mass.

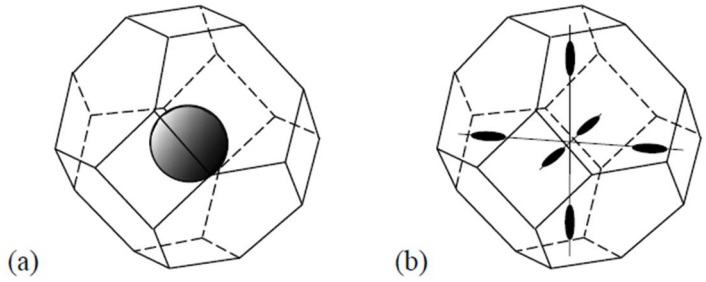

Figure (3.4.2) Constant electron energy surfaces in the Brillouin zones (space or k-space): (a) as spherical band such as GaAs; (b) an ellipsoidal band such as Si. Si has six identical conduction bands.

3.5 Fermi-Dirac Distribution

Although the classical free electron theory gave good results for electrical and thermal conductivities including Ohm's law in metals, it failed in certain other respects. These failure was eliminated by having the free electron obeys the Fermi-Dirac distribution. The ground state is state of the N electron system at absolute zero. What happens as the temperature is increased The solution is given by the

Fermi-Dirac distribution. The kinetic energy of the electron increases as the temperature is increased: some energy levels are occupied 11-8which were vacant at absolute zero, and some levels are vacant which were occupied at absolute zero (Figure 3.5.1). The Fermi-Dirac distribution fo gives the probability that an orbital at energy E will be occupied by an ideal electron in thermal equilibrium.

$$f_a = \frac{1}{e^{(E-E_F)k_BT} + 1} \qquad (3.5.1)$$

Figure (3.5.1) Fermi-Dirac Distribution at the Various Temperatures.

3.6 Electron Concentration

The electron concentration n in thermal non equilibrium is expressed as

$$n = \int_0^\infty g(E)f(E)dE \qquad (3.6.1)$$

where f(E) is the temperature-dependent occupation probability in thermal nonequilibrium. It becomes the Fermi-Dirac distribution $f_0(E)$ in thermal equilibrium as shown in Equation (3.5.1), which becomes unity at absolute zero when E is less than EF, and zero when E is greater than EF(Figure 11.5). The electron concentration n in thermal equilibrium is

$$n = \int_0^\infty g(E) f_0(E) dE \tag{3.6.2}$$

Using Equations (3.4.10) and (3.5.1), the electron concentration n in thermal equilibrium is

$$n = \frac{1}{2\pi^2}\left[\frac{2m_d^*}{\hbar^2}\right]^{\frac{3}{2}} \int_0^\infty \frac{E^{\frac{1}{2}}}{e^{(E-E_F)k_B T} + 1} \tag{3.6.3}$$

3.7 Fermi Energy in Metals

The Fermi-Dirac distribution implies that at absolute zero (in the ground state of a system) the largest Fermions (electrons, holes, etc.) are filled up in the density of states, of which the energy is often called the Fermi energy (Figure 3.7.1), but here we specifically redefine it as the Fermi energy at absolute zero. So that the Fermi energy is temperature-dependent quantity. It is sometimes called the Fermi level or the chemical potential. In general, the chemical potential (temperature dependent) is not equal to the Fermi energy at absolute zero. The correction is very small at ordinary temperatures (under an order of 10^3K) in ordinary metals.

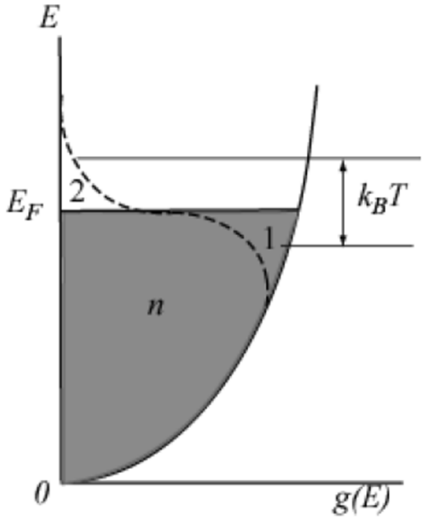

Figure (3.7.1) Electron concentration n is given by the area under the density of states curve up to the Fermi energy EF. The dashed curve represents the density of filled orbitals at a finite temperature. The electrons are thermally excited from region 1 to region 2.

The largest number of states N can be defined when a sphere of Fermi radius k_F is divided by the smallest volume $\left(\frac{2\pi}{L}\right)^3$ in k-space (see Figure 3.3.1).

$$N = \frac{2.\frac{4}{3}\pi k_F^3}{\left[\frac{2\pi}{L}\right]^3} \tag{3.7.1}$$

where the factor of 2 accounts for the Pauli Exclusion Principle. Since the crystal volume is defined as V = L3, the Fermi wave vector is

$$k_F = \left[\frac{3\pi^2 N}{V}\right]^{\frac{1}{3}} = (3\pi^2 n)^{\frac{1}{3}} \tag{3.7.2}$$

where N/V is the electron density (or electron concentration) n at the Fermi surface, which can be obtained from the lattice points, the lattice constant and the mass of the atom (n is usually a great number of about 10^{22} cm-3). The Fermi wave vectors form the Fermi surface, which separates the occupied from the unoccupied levels. The Fermi surface is one of the fundamental constructions in the modern theory of metals; in general it is not spherical. The Fermi energy is

$$E_F = \frac{\hbar^2}{2m}(3\pi^2 n)^2 \tag{3.7.3}$$

or the electron concentration n is

$$n = \frac{2(2m)^{1/2}}{3\pi^2\hbar^3} E_F^{3/2} \tag{3.7.4}$$

This can be also obtained by integrating Equation (3.6.3) from zero to EFwith $f_0 \approx 1$for $(E - E_F)k_BT << 0$ in most metals. The Fermi velocity at the Fermi surface is

$$v_F = \frac{\hbar k_F}{m} = \frac{\hbar}{m}(3\pi^2 n)^{\frac{1}{3}} \tag{3.7.5}$$

For metals, the Fermi velocity is an order of 10^8 cm/s. This is a substantial velocity (about 1 percent of the speed of light). From the view point of classical statistical mechanisms, this is quite a surprising result, for we are describing the ground state (T = 0), and all particles in a classical gas have zero velocity at T = 0 (classical equipartition energy$1/2mv^2 = 3/2kBT$). The Fermi velocity is only an approximation to the average electron velocity; this approximation works best in metals and in heavily doped semiconductors. The electron mean free path A can be approximated by

$$A \approx v_F\tau \tag{3.7.6}$$

Where is τ the relaxation time. The mean free path is a measure of the average distance between successive scattering events. The relaxation time is the average time between successive collisions. The wavelengthλ of electrons may be estimated by the de Broglie expression.

$$\lambda = \frac{h}{p} \approx \frac{2\pi\hbar}{mv_F} \tag{3.7.7}$$

3.8 Fermi Energy in Semiconductors

In semiconductors, we usually have$(E - E_F)/k_BT >> 1$, and then $(E - E_F)/k_BT$becomes much greater than 1. Therefore, eliminating one we have

$$f_a = \frac{1}{e^{(E-E_F)k_BT} + 1} = \exp\left[-\frac{E - E_F}{K_BT}\right] \tag{3.8.1}$$

The electron concentration n in equilibrium from Equation (3.7.4) is

$$n = \frac{1}{2\pi}\left[\frac{2m_d^*}{\hbar^2}\right]^{3/2} \int_0^\infty \exp\left[-\frac{E - E_F}{K_BT}\right] dE \tag{3.8.2}$$

This can be solved using Gamma function. The electron concentration n in single band is reduced to (this is known as the Boltzmann approximation)

$$n = N_v 2\left[\frac{2m_d^* K_BT}{2\pi.\hbar^2}\right]^{3/2} \exp\left[\frac{E_F}{K_BT}\right] \tag{3.8.3}$$

where N_v is the degeneracy (number of bands or valleys having the same band edge energy and the same wave vector). For example, Si has the degeneracy of six valleys (see Figure (3.7.1). Solving forE_F, we have

$$E_F = K_BT \ln\left[\frac{n}{2N_v}\left[\frac{2m_d^* K_BT}{2\pi.\hbar^2}\right]^{-\frac{3}{2}}\right] \tag{3.8.4}$$

In typical semiconductors, the Fermi energy EF may be below the conduction band edge EC. The band gap Egis the difference between EC and EV, which is usually much larger than $k_BT$as shown in Figure (3.7.1) the electron concentration n is the shaded area under the density of states curve and the Fermi energy at room temperature. Note that the Fermi energy greatly affects the electron concentration n in the conduction band, which is much smaller than that of a metal (Figure 3.8.1).

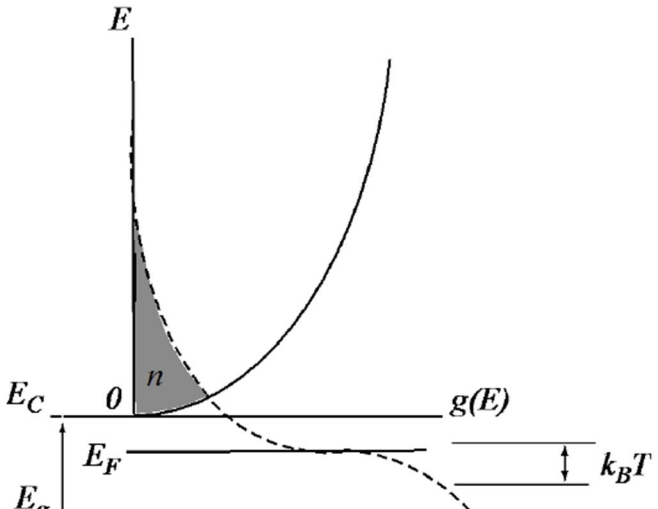

Figure (3.8.1) Electron concentration n in a semiconductor is given by the area under the density of states curve and the Fermi energy EF at room temperature. The Fermi energy EF is located under the minimum of conduction band. The dashed curve represents the density of filled orbitals at a finite temperature.

3.9 Energy Bands

The free electron model of metals gives us good insight into the electrical conductivity and electrodynamics of metals. But the model fails to help us with other questions, for example the relation of conduction electrons in the metal to the valence electrons of free atoms and many transport properties. Every solid contains electrons. The important question for electrical conductivity is how electrons respond to an applied electric field. We shall see that electrons in crystals are arranged in energy bands separated by regions in energy for which no wavelike electron orbits exist. Such forbidden regions are called energy gaps or band gaps (E_G) which are shown in Figure 3.8.1 wherein the differences between a metal, a semiconductor and an insulator are summarized schematically.

The crystal behaves as an insulator if the allowed energy bands are all either filled or empty, for then no electrons can move in an electric field. The crystal behaves as a metal if one or more bands are partly filled. The crystal is a semiconductor or semimetal if one or two bands are slightly filled or slightly empty.

To understand the difference between insulators and conductors, we must extend the free electron model to take account of the periodic lattice of the solid. The possibility of a band gap is the most important new property that emerges.

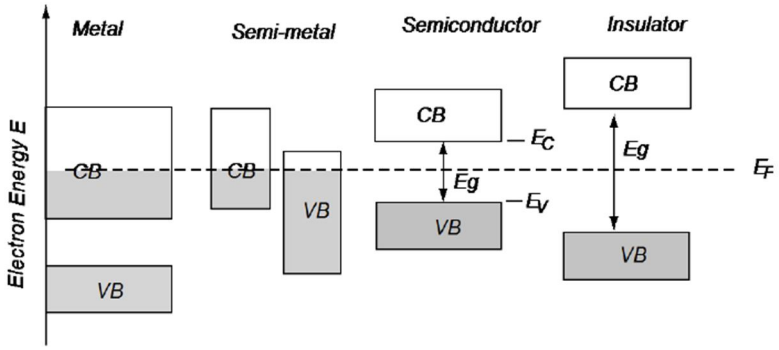

Figure (3.9.1) Energy level diagrams for a metal, a semiconductor, and an insulator. Metals have a partly occupied band (shaded).

For semiconductors and insulators, the Fermi level lies between the occupied valence band and the unoccupied conduction band.

3.10 Multiple Bands

There may be two separate bands: a conduction band for electrons and a valence band for holes as shown in Figure 3.10.1(a). In many semiconductors such as Si and PbTe, there may be also multiple bands that have the same energy levels, whereby it is called degeneracy. The heavy and light holes are degenerate and the split-off hole in the valence band is slightly off the valence band edge (maximum).

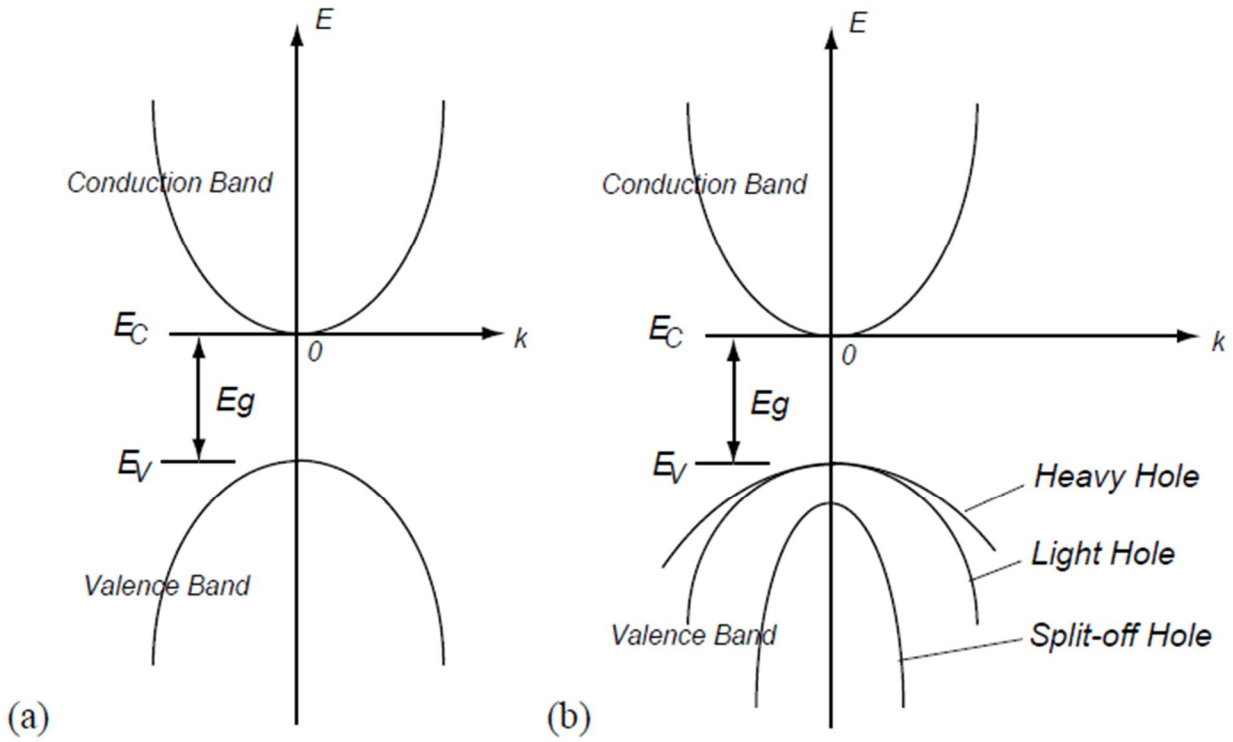

Figure (3.10.1) Band structures of a semiconductor including the conduction band and the valence bands. (a) A model of a conduction band and a valence band, and (b) a model of multiple bands.

3.11 Direct and Indirect Semiconductors

The type of band gap in semiconductors is important for the selection of material for many electronic devices including thermoelectric devices, solar cells and lasers. There are two types of band gaps in semiconductors, which are direct and indirect band gap. The energy E of a particle is always associated with a wave vector k (or momentum), which implies that, for any transition between bands, both energy and momentum must be conserved. When an electron absorbs enough energy to exceed the energy gap E_g, the electron can jump from the valence band into the conduction band. The source of the energy could be photons, phonons, or electric field.

In direct band gap semiconductors, such as GaAs, the maximum and minimum of energy versus momentum relationship occur at the same value of the wave vector (Figure 3.10.1 (a)). In indirect band gap semiconductors like Si and Ge, the maximum and minimum of the energy versus momentum relationship occurs at different wave vectors, which is pictured in Figure 3.10.1 (b). In this case, the electron cannot directly jump into the conduction band, but once the electron at the valence band edge EV absorbs energy (photon, phonon, or electric field) and reaches the energy level of the conduction band edge EC across the energy band Eg, it can indirectly jumping to the conduction band with the aid of phonon energy because phonon usually exists anyway.

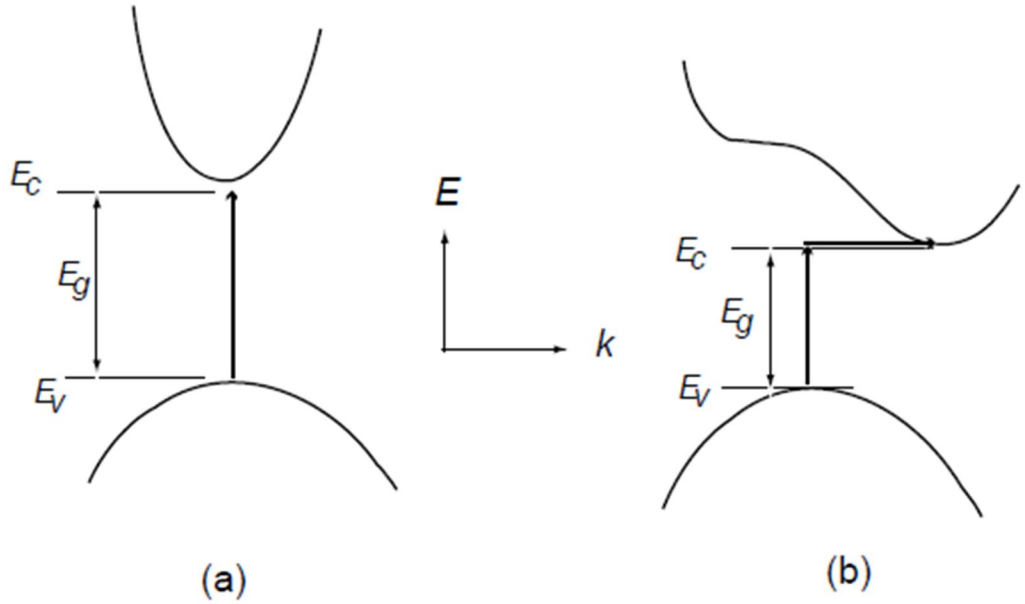

Figure (3.12.1) Energy versus wave vector diagrams in (a) direct band gap and (b) indirect band gap semiconductors.

Direct and indirect gap semiconductors have major differences in their optical properties. Direct band gap semiconductors are more efficient photon emitters, semiconductor lasers are made of direct gap semiconductors such as GaAs,

whereas most electronic devices including thermoelectric devices are built on indirect semiconductors.

3.12 Periodic Potential (Kronig-Penney Model)

So far we have dealt with a free electron. In fact the electron in a crystal experiences a periodic potential which is along a line of the ionized atoms. Assuming one-dimensional lattice with the lattice constant a as shown in Figure 3.12.1 (a), resembling the individual atomic potentials as the atom is approached closely and flattening off in the region between atoms. We approximate this by a square periodic potential in Figure 3.12.1 (b) as introduced by Kronig and Penney.

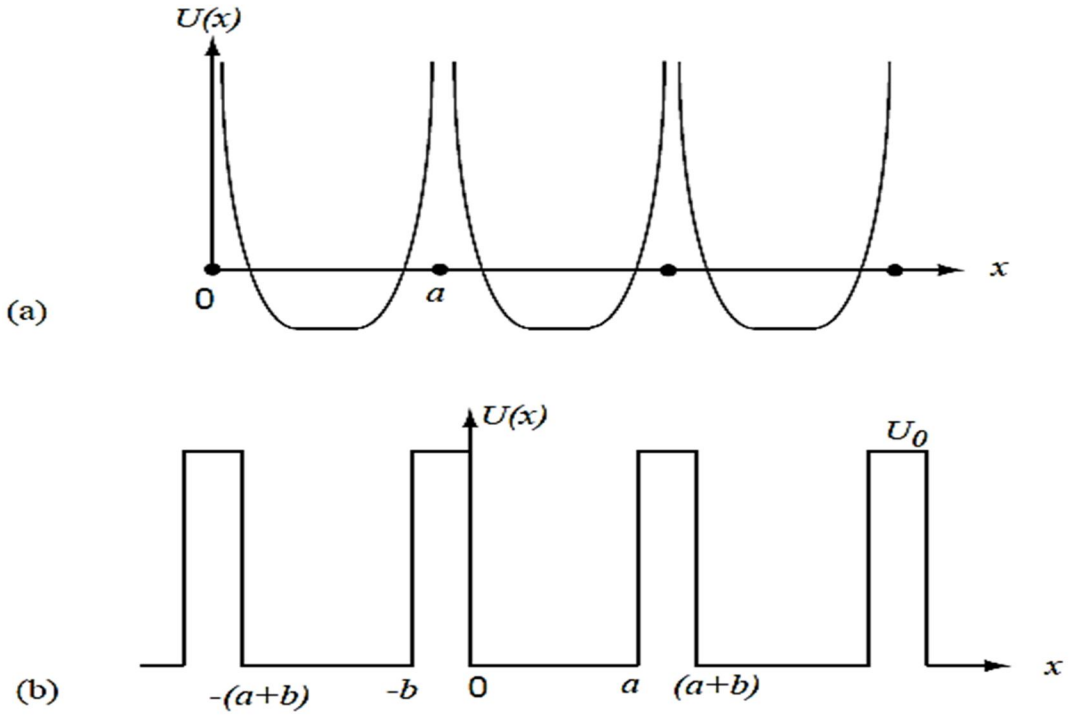

Figure (3.12.1) periodic potential energy model of kroingpenny model.

The Schrodinger equation for the wave function is then

$$-\frac{\hbar^2}{2m}\frac{\partial^2\psi}{\partial x^2} + (U(x) - E)\psi = 0 \qquad (3.12.1)$$

The potential distribution is given by

$$U(x) = \begin{cases} 0 & for\ 0 < x \leq a \\ U_0 for - b \leq x \leq 0 \end{cases} \quad (3.12.2)$$

Subject to the following periodicity requirement

$$U(x + a + b) = U(x) \quad (3.12.3)$$

The general solutions for Equation (11.42) are

$$\psi = Ae^{ik_x} + Be^{ik_x} \quad (3.12.4)$$

$$\psi = Ce^{Q_x} + De^{Q_x} \quad (3.12.5)$$

where

$$E = \frac{\hbar^2 k^2}{2m} and U_0 - E = \frac{\hbar^2 Q^2}{2m} \quad (3.12.6)$$

And K and Q are to be determined, from which the Eigen energy E of the electron inside such a periodic potential is to be extracted.

Four boundary conditions are needed to determine the unknown coefficient A, B, C, and D. We can use the continuity of the wave function and its derivative at x = 0, which gives

$$A + B + C + D \quad (3.12.7)$$

$$iK(A - B) = Q(C - D) \quad (3.12.8)$$

Two more boundary conditions are necessary to determine the four unknown coefficients. Due to the periodicity in the potential, the wave function at any two points separated by a lattice vector is related through the Bloch theorem in the x-direction,

$$\psi(x + a + b) = \psi(x)e^{ik(a+b)} \quad (3.12.9)$$

We should distinguish the wave vector k from the propagation vector of the solution K in Equation (3.12.4). The latter contains the energy of the electrons that we want to find. We want to find a relation between k and E, which is equivalent to

a relation between k and K. The continuity requirements for the wave function and its derivative at x = a are then

$$Ae^{ik_a} + Be^{ik_a} = (Ce^{Q_b} + De^{Q_b})e^{ik(a+b)} \qquad (3.12.10)$$

$$ik\left(e^{ik_a} + Be^{ik_a}\right) = Q(Ce^{Q_b} + De^{Q_b}) \qquad (3.12.11)$$

Four equations with four unknowns have a solution only if the determinant of the coefficients vanishes, yielding

$$\frac{Q^2 - k^2}{2KQ}\sinh(Qb)\sin(ka) + \cosh(Qb)\cos(ka) = \cos\left(k(a+b)\right) \qquad (3.12.12)$$

It is rather tedious to obtain this equation. The result is simplified if we represent the potential by the periodic delta function obtained when we pass to the limit b = 0 and $U_0 = \infty$in such a way that $Q^2ba/2 = P, a$, a finite quantity. In this limit $Q >> K$ and $Qb << 1$. Then, Equation (3.12.12) reduces to

$$\frac{P}{ka}\sin(Ka) + \cos(Ka) = \cos(ka) \qquad (3.12.13)$$

The range of K for which this equation has solutions are plotted in Figure 3.12.1, for the case P = $3\pi/2$. We can convert the solution for K into energy, and redraw the graph as a function of ka as shown in Figure 3.12.2 The figure shows that, for each wave vector k, there are multiple values for the electron energy E.

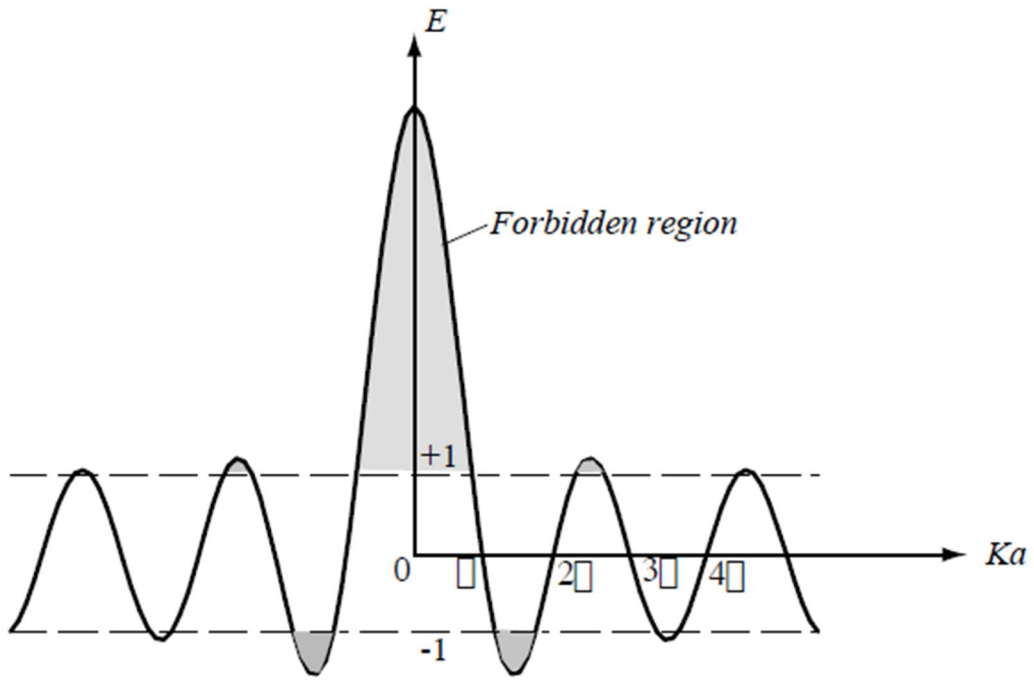

Fig (3.12.2): Forbidden region

Figure (3.12.2) Left-hand side of Equation (3.12.13) as function of Ka. Because the right-hand side is always less than or equal to one, there are regions (the shaded area) where no solution for Ka exists, and thus no electrons exist with energy corresponding to the values of K in these regions.

The electron energy forms quasi-continuous bands (because k itself is quasi-continuous) separated from each other by a minimum gap that occurs at ka = sπ(s = 0, ±1, ±2, …), or k = sπ/a, at which the right-hand side of Equation (3.12.2) is ±1. Figure 3.12 (b) implies that there are multiple values of k for each E. However, the Bloch theorem says that wave functions corresponding to the wave vectors k separated by m (2π/a) (since b = 0) are identical, they are the same quantum state and should be counted only once. Thus, rather than plotting the energy Eigen values for all the wave vectors, we can plot them in one period, as shown in Figure 3.12.3 This way of representation is called the reduced-zone representation. The relationship between the energy and the wave vector is the dispersion relation.

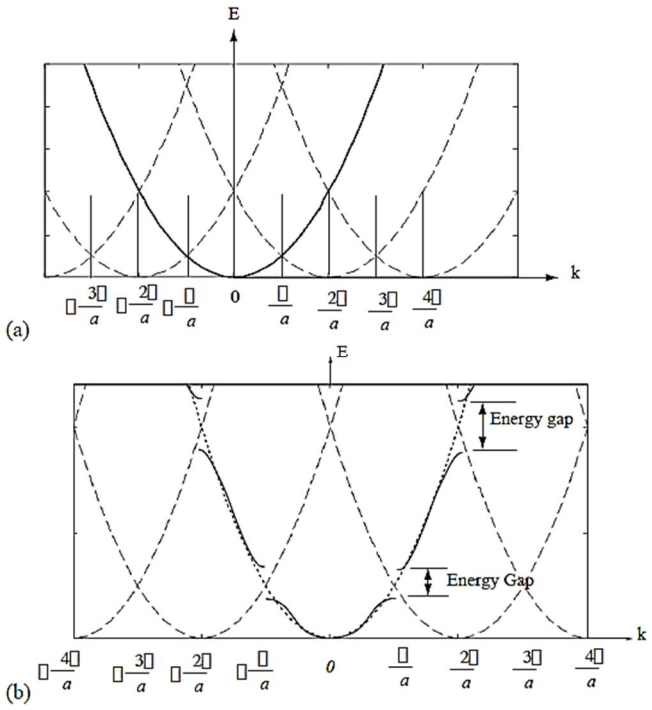

Fig 3.12.3 Parabolic energy curves of a free electron in one dimension

Figure (3.12.3) (a) Parabolic energy curves of a free electron in one dimension, periodically continued in reciprocal space. The periodicity in real space is a, and (b) extended zone: splitting of the energy parabola at the boundaries of the first Brillion zone. The energy gaps are forbidden regions. The solid lines from Kronig-Penney model.

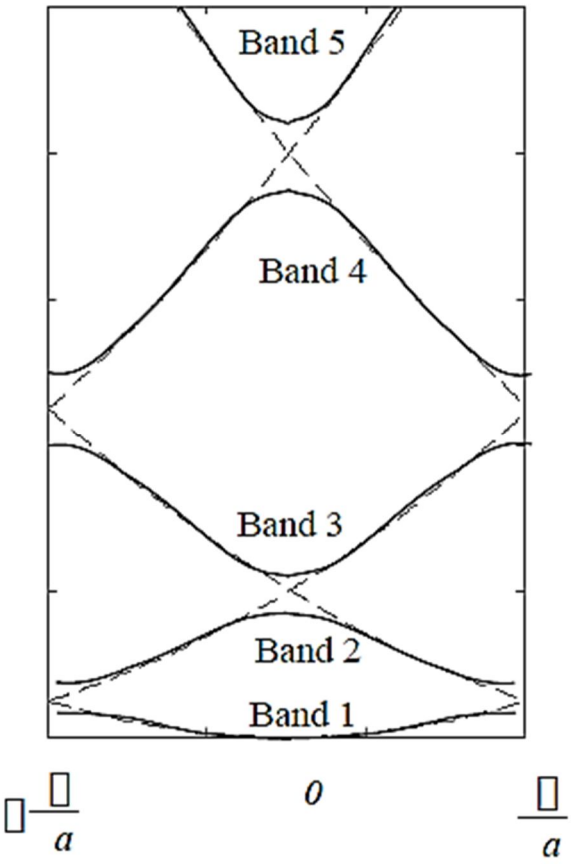

Figure (3.12.4) The solid lines show the energy bands in the reduced zone.

The free electron dispersion relations are shown as dashed lines.

The ab initio calculated electronic band structure using the density functional theory (DFT) depicted in Figure 3.12.4 shows the indirect energy gap and the threefold degeneracy of the valence band at the Fermi energy. It is seen that the approximate sum of the energy bands for a specific energy level in Figure 3.12.5 (a) corresponds to the density of states for the energy level in Figure 3.12.5 (b). From this approach, we can estimate the effective mass using Equation (3.12.13) that is the second derivative of energy with respect to wave vector. Also we obtain the band gap from the figure.

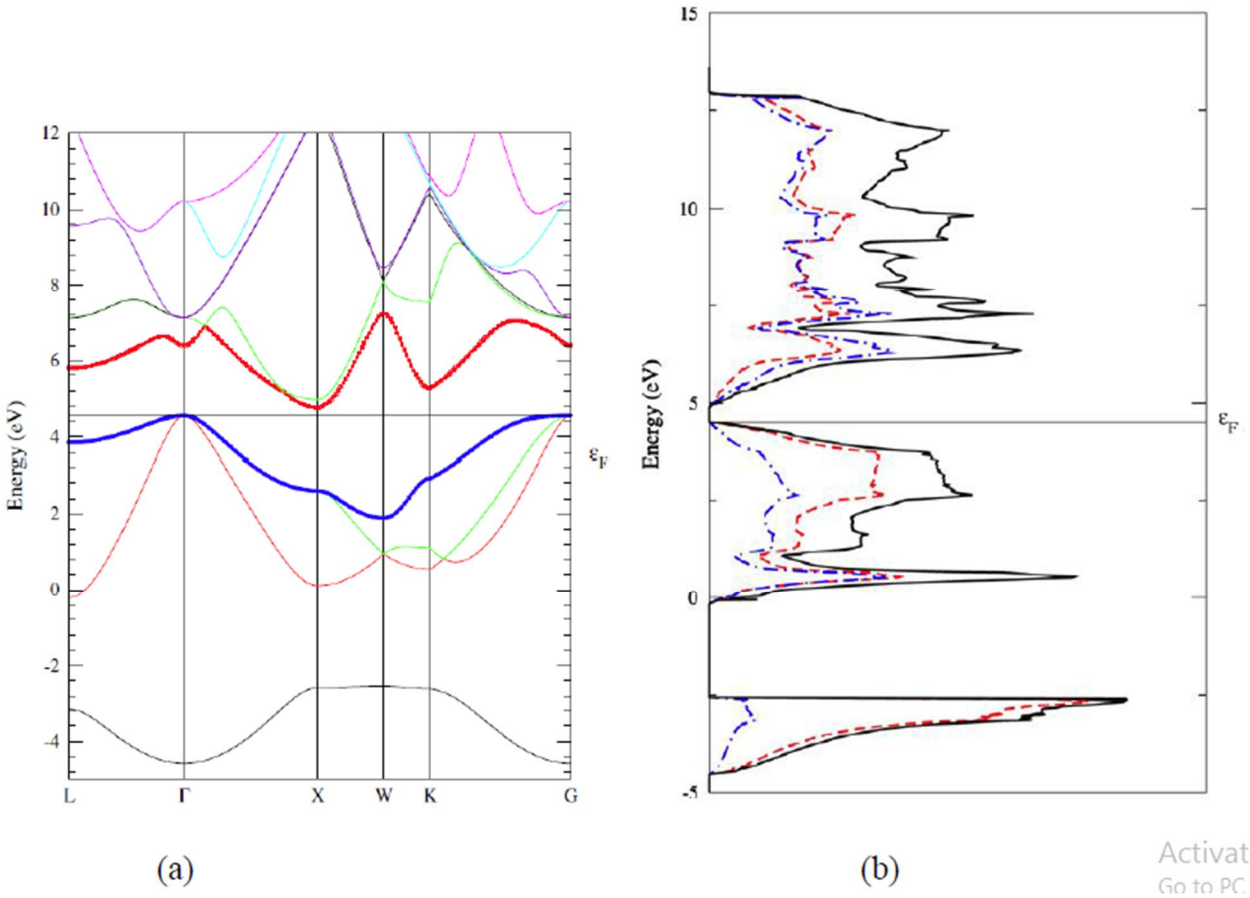

Figure(3.12.5) (a) Electronic band structure of Mg2Si calculated with the density functional theory (DFT), and (b)

Electronic band structure of Mg2Si calculated with the density functional theory (DFT), and (b) total electron density of states (DOS) projected on magnesium and silicon atoms, the solid line for total DOS, the dashed line for silicon contribution, and the dot-dashed line for magnesium contribution. Bullet at al. (2011)

3.13 Effect of temperature on Fermi level:

The Fermi temperature is defined as the temperature corresponding to the Fermi energy such that:

$$E_f = K_b T_f \qquad (3.13.1)$$

With the Fermi energy of the order of a few eV, the Fermi temperature works out to be of the order of several thousand Kelvin (approximately 10,000 K).How do we reconcile the fact that the material is at room temperature or lower, or even at 0 Kelvin, while the Fermi temperature is 10,000 K? One way to look at the situation is as follows: When we measure the temperature of a material, we do not typically measure the temperature of a single atom or electron. What we measure is the average temperature of the material. There is invariably going to be a distribution Of energy within the material. In this distribution, an extremely small thermal mass, consisting ofa very small fraction of the nearly free electrons (which is itself a very small fraction of the total electrons in the system), is at the Fermi energy, and the temperature corresponding to that energyis the relatively high Fermi temperature. Therefore the „high" Fermi temperature is not inconsistent with the „low" temperature or the solid as a whole.

Chapter Four

Material and Methods

4.1 Introduction

In this chapter one propose a simple and low-cost experimental set-up through which chapter one can demonstrate the Seebeck effect using a thermocouple and an instrumentation amplifier. The experiment can be set up and conducted during a 1-hour laboratory session.

4.2 The experiment

For demonstration of experimental work, one set up the thermocouple circuit was set up which was shown in Figure (4.3.1) and it is provides a list of the major components used in the set-up. includes two J-type thermocouples, each consisting of a pair of iron and constantan wires that are welded at one end. One of the thermocouples is used for measuring the reference temperature (T R_{ef}), while the other thermocouple is used for measuring the ambient temperature (T). To make the connection between the constantan wires of each thermocouple, we simply twisted them together. Since the magnitude of the Seebeck voltage generated in the setup is of the order of a few μV, an instrumentation amplifier was used to amplify the magnitude of the voltage.

4.3 The Material

Three thermocouple Al-Fe, Fe-Cu and Cu-Al were fabricated. one end of thermocouple can be heated by a heater the temperature of each end can be measured by thermometer. the voltmeter reading in the range of mv is used to determine the electromotive force of the thermocouple.

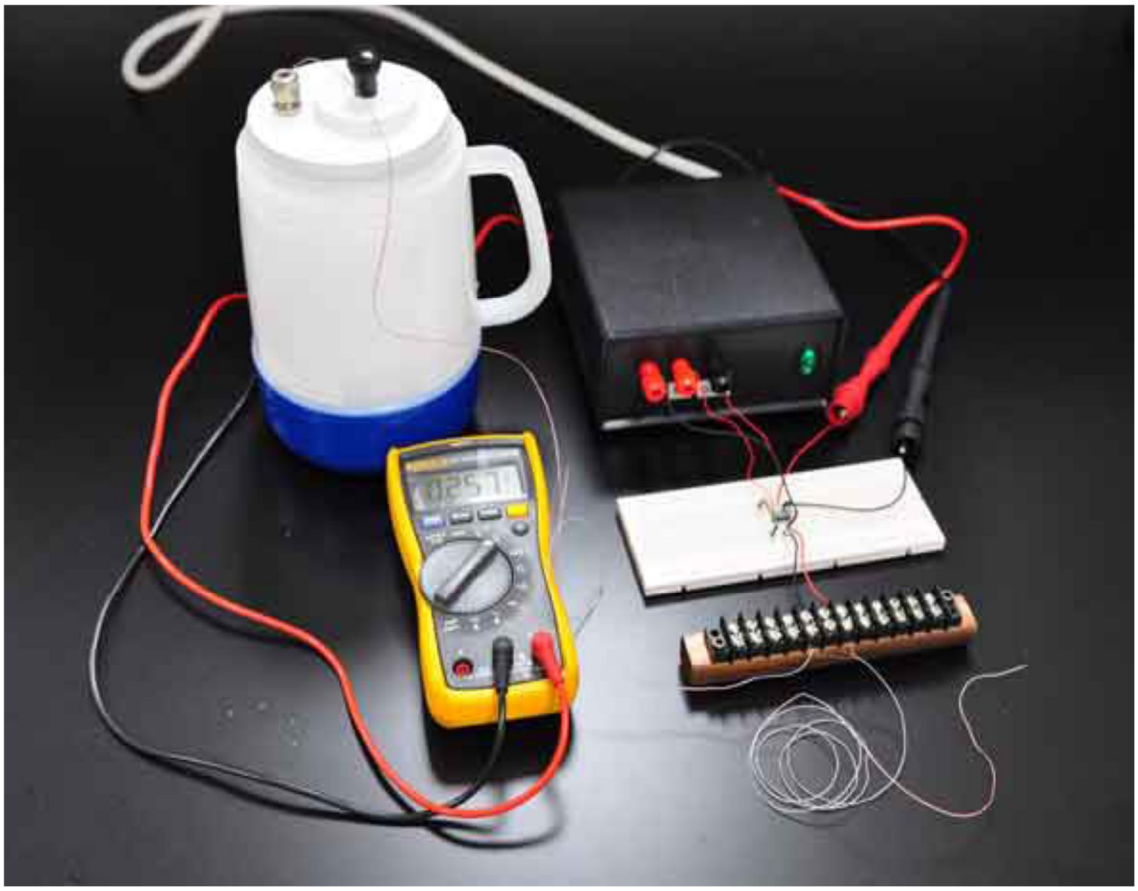

Figure (4.3.1) shows the Equipment's and the Circuit Used for Measurements

4.4 Results:

The relations between induced EMF and temperature change of one end of Al/Cu, Fe/Al and Cu/Fe thermocouples were recorded, in table 4.4.1, 4.4.2 and 4.4.3 all experiments one end is kept at room temperature 30^0.

Table (4.4.1) Induced voltage EMF V as a function of temperature θ o f the other end of thermocouple for Al/Cu

$T(C^o)$	$V(V)$
40.570	0.134
53.053	0.158
60.013	0.182
67.799	0.214
78.729	0.237
89.608	0.264
99.713	0.293
110.643	0.303
119.202	0.329
130.081	0.360
139.413	0.379
149.518	0.410
161.995	0.422
168.234	0.454
179.886	0.477
189.218	0.487
199.324	0.497

Table (4.4.2) Induced voltage EMF V as a function of temperature θ o f the other end of thermocouple for Fe/Al

$T(C^o)$	$V(V)$
39.854	0.592
50.939	0.672
60.477	0.766
69.448	0.892
80.018	1.033
90.639	1.159
101.208	1.200
110.179	1.360
119.151	1.500
129.771	1.573
139.774	1.646
149.312	1.740
159.881	1.860
170.451	1.886
180.505	1.993
190.043	2.026

Table (4.4.3) Induced voltage EMF V as a function of temperature θ o f the other end of thermocouple for Cu/Fe

$T(C^o)$	$V(V)$
40.359	0.196
48.849	0.222
59.124	0.258
70.705	0.301
78.760	0.331
89.906	0.372
99.745	0.438
109.106	0.497
120.295	0.571
129.656	0.592
140.366	0.635
150.206	0.668
159.566	0.706
168.492	0.730

4.5 Discussion:

Thermocouple induced EMF depends strongly on the difference in temperature between the two ends of the thermocouple.

In view of figures (4.4.1) (4.4.2) and (4.4.3) for AL/Cu ,Fe/AL ,and Cu/Fe all thermocouples it is clear that the induced EMF is directly proportional to temperature this can be explained if one assumes that the induced EMF v is related to the thermal kinetic energy gained by the electrons due to heating effects, i.e eV = electron kinetic energy = $\frac{1}{2}mv^2$ but according to kinetic theory

$$\frac{1}{2}mv^2 = E = \frac{3}{2}KT \qquad (4.5.2)$$

Inserting (4.4.1) in (4.4.2) yields

$$V = \frac{3KT}{e} \qquad (4.5.3)$$

This relation can be displayed graphically in figure (4.4.1) comparing figures (4.4.1, 4.4.2) with (4.4.3), it is clear that the theoretical relation explain experimental

This result is similar to that used in explaining x-ray production where the applied voltage v causes electrons to acquire kinetic energy such that $eV = \frac{1}{2}mv^2$. The stopping potential in photoelectric effect also satisfies the same relation

4.6 Conclusions

Seebeck's EMF varies linearly with the temperature difference and its corresponding coefficient is a constant that does not depend on the temperature. According to the second Thomson relation there should not be Thomson heat for a linear effect. But yet, when charge carriers enter a wire at a cold end, and leave it at a hot end, their heat content changes and they must cool it or absorb heat from its vicinity.

Thermoelectric effects in systems are much more complicated than the simple model presented here. In metals only electrons with energy within a few kT around the Fermi energy contribute to the current, and their number is strongly temperature dependent, mainly at low temperatures. In addition, their thermal energy is not that of free particles. Yet, Seebeck effect and Pettier effect are basically reversible thermodynamic processes. Discussing them in terms of non-equilibrium irreversible theories is meaningless.

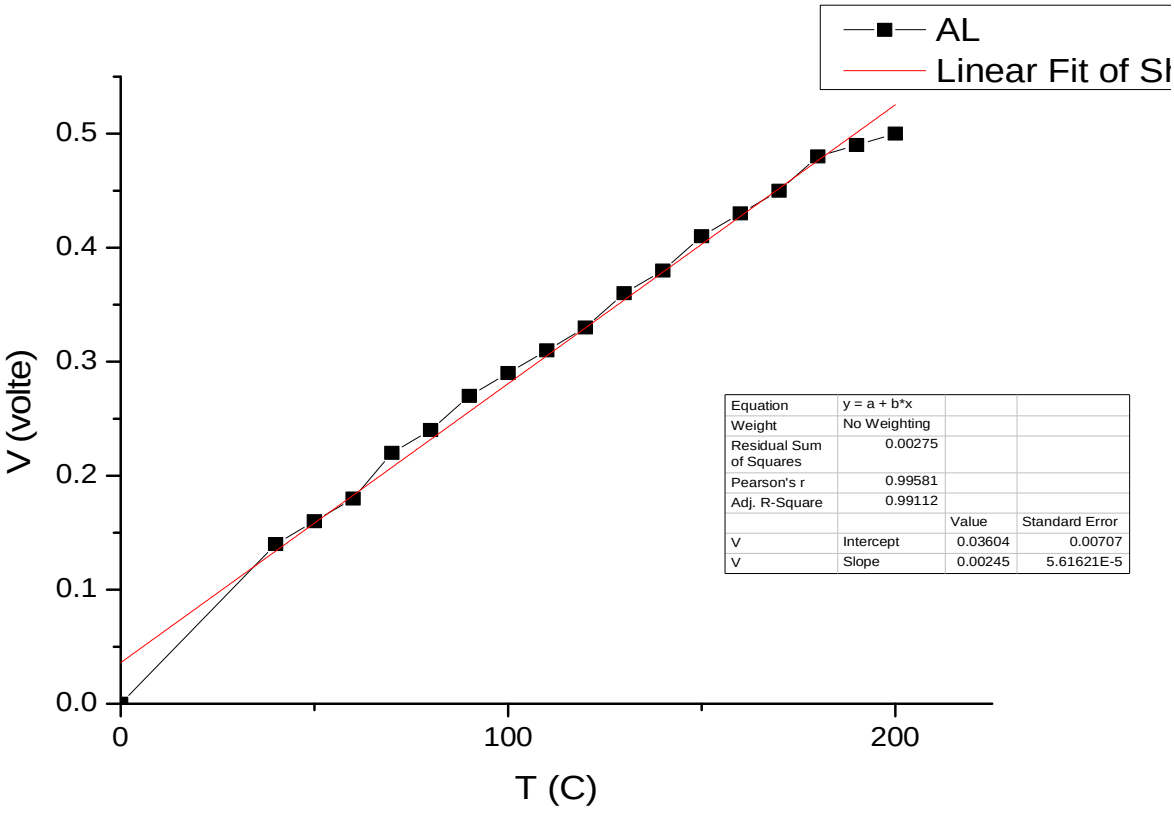

Figure (4.4.1) Relation between the EMF and Temperature for Al-Cu Alloy as Thermocouple

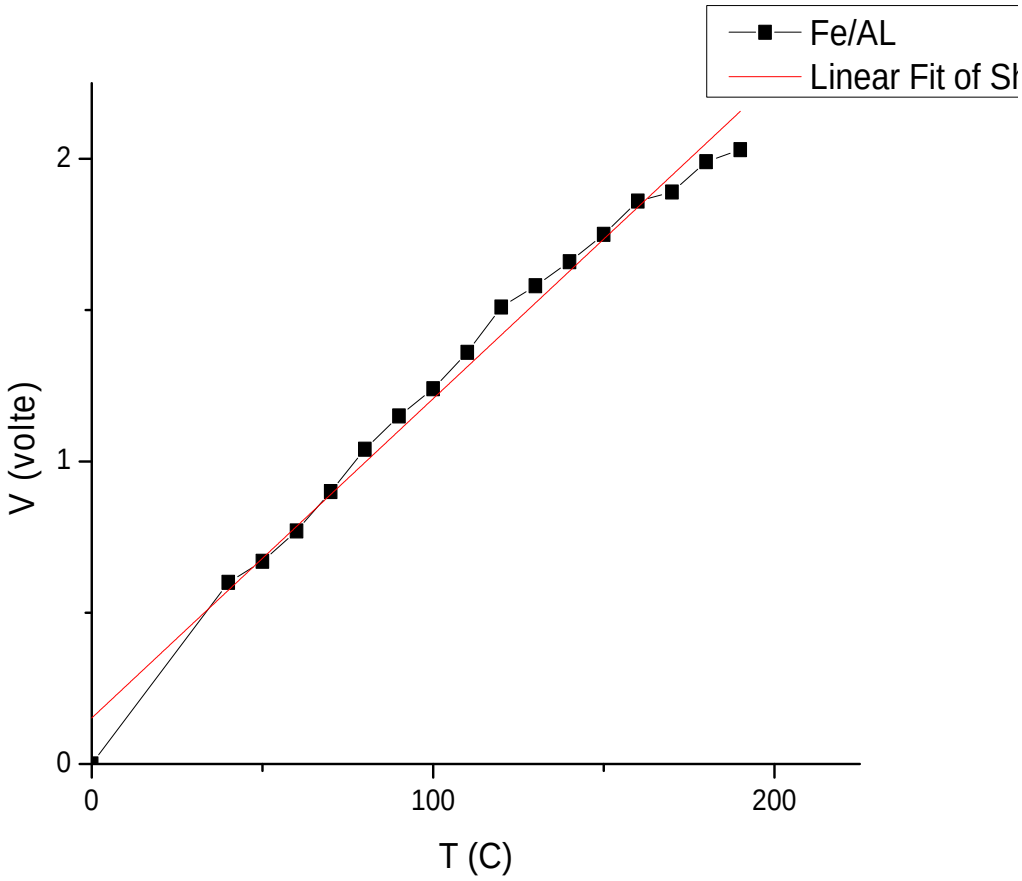

Figure (4.4.2) Relation between the EMF and Temperature for Al-Fe Alloy As Thermocouple

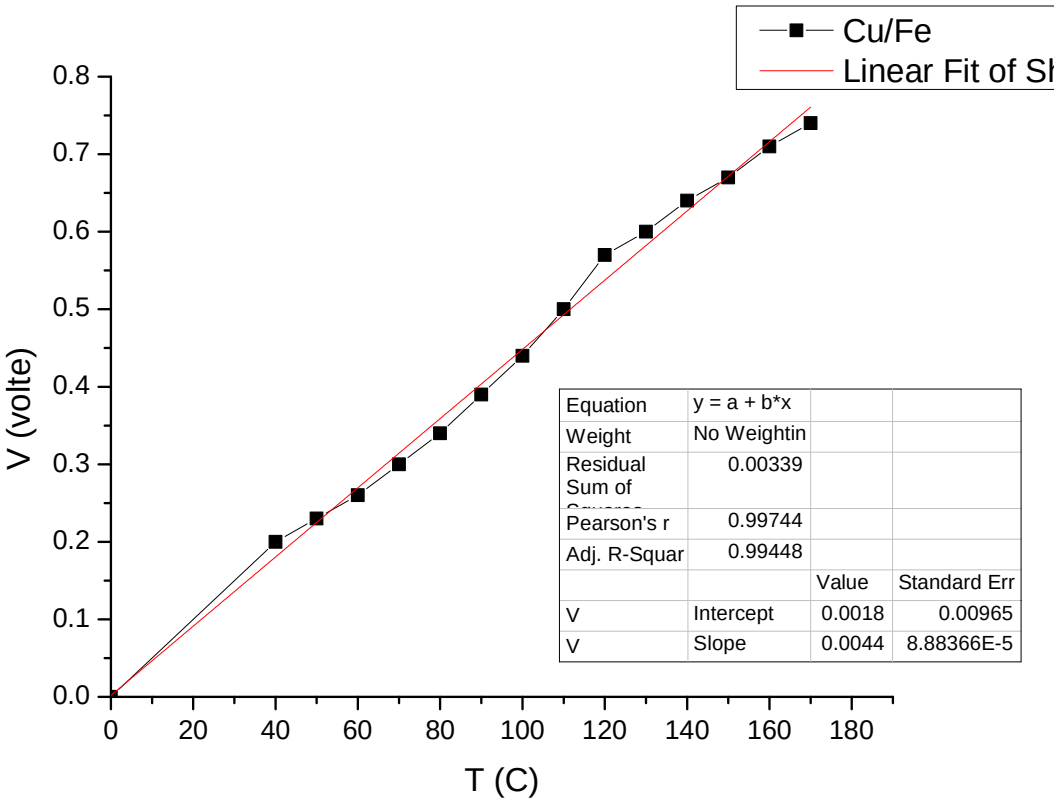

Figure (4.4.3) Relation between the EMF and Temperature for Fe-Cu Alloy as Thermocouple

4.7 Recommendations:

1. Seebeck effect it was important in new technological area so it needs more research program in this field.
2. The thermocouple not understood clearly in their applications while there was a wide field which can be used thermocouples.

4.8 References

[1] A.F. Ioffe, Semiconductor Thermoelements and Thermoelectric Cooling, Infosearch, London, 1957.

[2] W.M. Yim, F.D. Rossi, Solid State Electron. 15 (1972) 1121–1140.

[3] H.J. Goldsmid, in: T.M. Tritt (Ed.), Semiconductors and Semimetals, vol. 69, Academic Press, New York, 2001,p. 1.

[4] E.A. Skrabek, D.S. Trimmer, in: D.M. Rowe (Ed.), CRC Handbook of Thermoelectrics, CRC Press, Boca Raton,1994.

[5] B. Abeles, D.S. Beers, G.D. Cody, J.P. Dismukes, Phys. Rev. 125 (1) (1962) 44–46.

[6] D.M. Rowe, C.M. Bhandari, in: Rhinehart Holt, Winston (Eds.), Modern Thermoelectrics, London, 1983.

[7] G.A. Slack, in: H. Ehrenreich, F. Seitz, D. Turnbull (Eds.), Solid State Physics, Academic Press, New York, 1979.

[8] D.G. Cahill, H.E. Fischer, S.K. Watson, R.O. Pohl, G.A. Slack, Phys. Rev. B. 40 (5) (1989) 3254–3260.

[9] S. Yamanaka, K. Kurosaki, A. Kosuga, K. Goto, H. Muta, Proc. Mat. Res. Soc. (Fall) (2005).

[10] G.S. Nolas, J.L. Cohn, G.A. Slack, Phys. Rev. B 58 (1998) 164.

[11] K. Hoang, S.D. Mahanti, J. Androulakis, M.G. Kanatzidis, Proc. Mat. Res. Soc. (Fall) (2005).

[12] R.F. Service, Science (2006) 1860.

[13] H. Bottner, G. Chen, R. Venkatasubramanian, Mat. Res. Soc. Bulletin 31 (2006) 211–217.

[14] A. Sommerfeld, Zeits. F. Physik 47 (1) (1928).

[15] A. Sommerfeld, N.H. Frank, Rev. Modern Phys. 3 (1) (1931) 1–8.

[16] F. Bloch, Zeits. F. Physik 52 (1928) 555.

[17] A.H. Wilson, Proc. Roy. Soc. London (A) 133 (822) (1931) 458–491.

[18] Bronstein, Phys. Z. Sowjetunion 2 (1932) 28.

[19] R.H. Fowler, Proc. Roy. Soc. London (A) 140 (842) (1933) 505–522.

[20] A.H. Wilson, Theory of Metals, Cambridge University Press, 1953.

[21] V.A. Johnson, K. Lark-Horovitz, Phys. Rev. 92 (2) (1953) 226–232.

[22] K. Lark-Horovitz, Middleton, Miller, Scanlon, Walerstein, Phys. Rev. 69 (1946) 259.

[23] Kelvin Lord, (Sir. W. Thomson) Collected Papers I, Cambridge University Press, 1882.

[24] L. Onsager, Phys. Rev. 37 (1931) 405.

[25] H.B. Callen, Phys. Rev. 73 (11) (1948) 1349–1358.

[26] H.P.R. Frederikse, Phys. Rev. 92 (2) (1953) 248–252.

[27] P.J. Price, Phys. Rev. 104 (5) (1956) 1223–1239.

[28] J. Tauc, Phys. Rev. 95 (6) ()(1954) 1394.

[29] L.E. Gurevich, J. Phys. (USSR) 9 (4) (1946) 26.

[30] R.P. Chasmar, R. Stratton, J. Electron. Control 7 (1959) 52–72.

[32] A. Asenov, J.R. Watling, A.R. Brown, D.K. Ferry, J. Comput.Elect. 1 (2002) 503–513.

[33] T.W. Tang, B. Wu, Semi. Sci. Tech. 19 (2004) 54–60.

[34] B. Yang, W.L. Liu, J.L. Liu, K.L. Wang, G. Chen, Appl. Phys. Lett. 81 (19) (2002) 3588–3590.

[35] R. Muller, T. Kamins, M. Chan, Device Electronics for Integrated Circuits, Wiley, New York, 1986.

[36] B. Yang, J.L. Liu, K. Wang, G. Chen, Proc. Mat. Res. Soc. 691 (2002) G.3.2.1–2.6.

[37] B. Yang, J.L. Liu, K.L. Wang, G. Chen, Appl. Phys. Lett. 80 (10) (2002) 1758–1760.

[38] W.L. Liu, T.B. Tasciuc, J.L. Liu, K. Taka, K.L. Wang, M.S. Dresselhaus, G. Chen, Intl. Conf. on Thermoelectrics,

2001, pp. 340–343.

[39] R. Venkatasubramanian, T. Colpitts, E. Watko, D. Malta, Proc. Spring Meet. Mat. Res. Soc. (1997).